This article was downloaded by: [Peter Monson]
On: 30 December 2014, At: 08:59
Publisher: Taylor & Francis
Informa Ltd Registered in England and Wales Registered Number: 1072954 Registered office: Mortimer House, 37-41 Mortimer Street, London W1T 3JH, UK

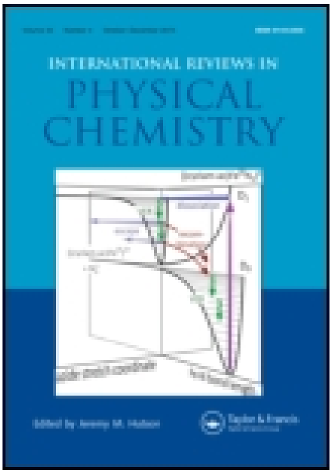

Click for updates

International Reviews in Physical Chemistry
Publication details, including instructions for authors and subscription information:
http://www.tandfonline.com/loi/trpc20

Modelling the assembly of nanoporous silica materials

Scott M. Auerbach[a][b], Wei Fan[b] & Peter A. Monson[b]
[a] Department of Chemistry, University of Massachusetts, Amherst, MA 01003, USA
[b] Department of Chemical Engineering, University of Massachusetts, Amherst, MA 01003, USA

Published online: 21 Dec 2015.

To cite this article: Scott M. Auerbach, Wei Fan & Peter A. Monson (2015) Modelling the assembly of nanoporous silica materials, International Reviews in Physical Chemistry, 34:1, 35-70, DOI: 10.1080/0144235X.2014.988038

To link to this article: http://dx.doi.org/10.1080/0144235X.2014.988038

PLEASE SCROLL DOWN FOR ARTICLE

Taylor & Francis makes every effort to ensure the accuracy of all the information (the "Content") contained in the publications on our platform. However, Taylor & Francis, our agents, and our licensors make no representations or warranties whatsoever as to the accuracy, completeness, or suitability for any purpose of the Content. Any opinions and views expressed in this publication are the opinions and views of the authors, and are not the views of or endorsed by Taylor & Francis. The accuracy of the Content should not be relied upon and should be independently verified with primary sources of information. Taylor and Francis shall not be liable for any losses, actions, claims, proceedings, demands, costs, expenses, damages, and other liabilities whatsoever or howsoever caused arising directly or indirectly in connection with, in relation to or arising out of the use of the Content.

This article may be used for research, teaching, and private study purposes. Any substantial or systematic reproduction, redistribution, reselling, loan, sub-licensing, systematic supply, or distribution in any form to anyone is expressly forbidden. Terms &

International Reviews in Physical Chemistry, 2014
Vol. 34, No. 1, 35–70, http://dx.doi.org/10.1080/0144235X.2014.988038

Modelling the assembly of nanoporous silica materials

Scott M. Auerbach[a,b], Wei Fan[b] and Peter A. Monson[b]*

[a]*Department of Chemistry, University of Massachusetts, Amherst, MA 01003, USA;* [b]*Department of Chemical Engineering, University of Massachusetts, Amherst, MA 01003, USA*

(*Received 14 September 2014; final version received 3 October 2014*)

We present a perspective on the molecular modelling of nanoporous silica material synthesis. We focus on two classes of materials: microporous zeolite materials in their all-silica forms, and ordered mesoporous silica materials. Several approaches have provided insight into the synthesis processes. These approaches range from quantum chemistry modelling of silica polymerisation to molecular simulations of ordered mesoporous silica assembly, and consider physical and chemical phenomena over several lengths and time scales. Our article focuses on models of porous silica material formation based on the assembly of corner-sharing tetrahedra, which we illustrate with applications to silica polymerisation, the formation of microporous crystals and the formation of ordered mesoporous materials. This is a research area where theoretical developments must closely align with experimentation. For this reason, we also devote a significant component of the present review to a survey of key developments in the experimental synthesis and characterisation of these materials. In particular, recent experiments have bracketed length scales of zeolite nuclei in the 5–10 nm range. On the other hand, recent molecular modelling work has accomplished the *in silico* self-assembly of both zeolitic and mesoporous materials within a unified modelling format. Our article serves to demonstrate the substantial progress that has been made in this field, while highlighting the enormous challenges and opportunities for future progress, such as in understanding the interplay of thermodynamics and kinetics in silica nanopore formation.

Keywords: nanoporous materials; zeolites; silica polymerisation; ordered mesoporous materials

Contents

---

*Corresponding author. Email: monson@ecs.umass.edu

1. Introduction

1.1. *Background*

In this review, we offer a perspective on the modelling of the synthesis of nanoporous materials. Such materials are of enormous importance in modern technology with applications in the chemical process industries, biomedicine and biotechnology, and also in microelectronics [1]. In chemical process industries, porous materials appear as catalysts and catalyst supports in adsorption and membrane separations processes [2,3]. In biomedicine and biotechnology, porous materials are used in chromatograpic separation, in sensors, and in tissue engineering [4–7]. In microelectronics, porous materials appear in optoelectronic devices and are used as low-k dielectric materials [8]. An ongoing theme in porous materials science and engineering is the tailoring of pore structure for specific applications. A classical example is the tailoring of channel dimensions in zeolites for shape-selective catalysis or separations. In developing new porous materials, an important goal is combining the tailoring concept in the context of materials that can offer a wide variety of pore structures, while exhibiting good thermal and chemical stability. Key to tailoring and controlling the formation of ordered nanoporous materials is gaining greater understanding of the mechanisms by which they form. Without such understanding, materials synthesis will remain a very slow, Edisonian process dominated by trial and error.

Silicate and aluminosilicate chemistry provide an enormously valuable route to stable nanoporous materials. In this article, we focus on two types of silica materials. In the first case, we deal with zeolites and related molecular sieves, which are crystalline inorganic framework oxides with nanometer-scale pores capable of discriminating molecules by shape, size and polarity [9]. Because of their potent catalytic activities, excellent hydrothermal stability and well-defined structures in the range of many molecules derived from petroleum and biomass, zeolites have been used extensively in a variety of chemical reactions to make fuels and fuel precursors. Zeolites have also been used as desiccants, ion exchangers and as materials for hydrogen and hydrocarbon storage. Figure 1 shows a schematic of the MFI framework structure showing the straight channel pore system within the zeolite crystal with a pore diameter of about 0.5 nm.

The framework topologies of zeolites are often understood in the language of hierarchical structure [10], which may offer a hint as to how zeolites form. In analogy with the hierarchical structure of proteins, zeolite structure can be understood in terms of the following hierarchy [9]:

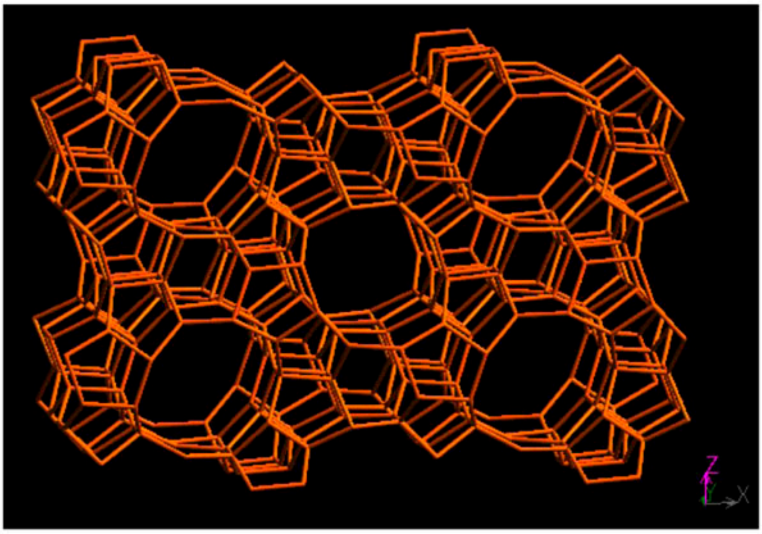

Figure 1. (Colour online) Visualisation of the MFI zeolite framework structure showing the straight channels with diameter of about 0.5 nm. Only shows Si atoms at vertices. (From Ch. Baerlocher and L.B. McCusker, Database of Zeolite Structures: http://www.iza-structure.org/databases/).
Note: MFI is a three-letter code that refers to the framework connectivity or topology. Examples of actual zeolite materials with the MFI topology are the aluminosilicate ZSM-5, and the all-silica zeolite silicalite.

- Primary: SiO_4/AlO_4 (TO_4) tetrahedra.
- Secondary: rings of alternating t/o atoms.
- tertiary: cages or channels.
- Quaternary: zeolite structures.

The utility of this notion is illustrated by the many zeolite topologies that can be constructed from, e.g. the sodalite cage (Figure 2). In particular, the SOD, LTA, FAU and EMT frameworks can all be constructed by connecting sodalite cages in different ways (Figure 2 shows this for FAU). Furthermore, atomic force microscopy [11] and high-resolution transmission electron microscopy [12] suggest that *existing zeolite surfaces* can grow in ‘quantized’ units of relatively high-order (e.g. tertiary) structures such as the double 6-ring shown in red in Figure 2.

On the other hand, there is very little evidence [13] to date that *zeolite nucleation* occurs through agglomeration of pre-formed, high-order structures. Instead, it appears that silica polymerisation yields amorphous nanoparticles or gels that eventually transform into zeolite nuclei through hitherto unknown processes referred to as ‘ageing’. While some progress has been made to elucidate this process as described below, it remains a grand challenge to develop advanced modelling and characterisation methods to identify the key species that participate in zeolite nucleation, and the critical transformations that eventually produce zeolite crystals.

The second type of material we focus on is the ordered mesoporous materials. Ordered mesoporous silica materials have been studied extensively since their discovery over two decades ago [14,15], because of their potential applications in catalysis and separations of species too large to fit in zeolite micropores. Ordered mesoporous silica

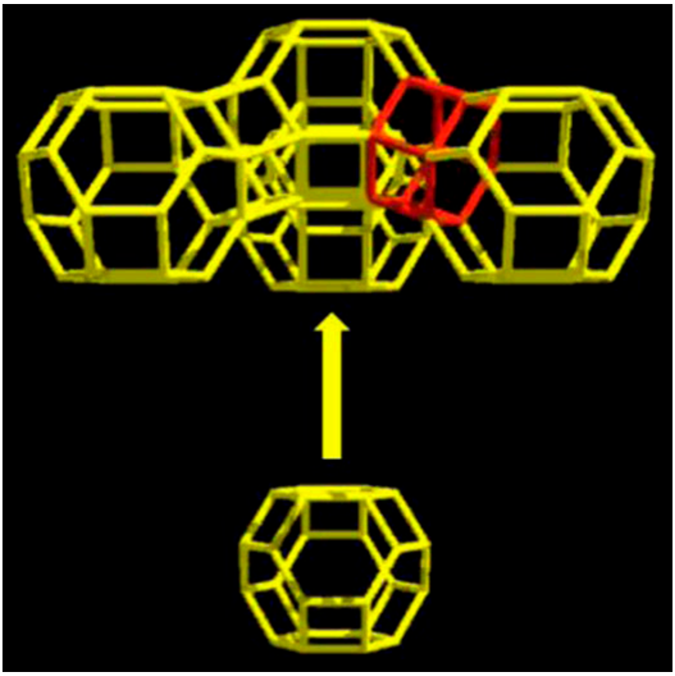

Figure 2. (Colour online) Conceptual construction of zeolite FAU by the addition of sodalite cages.

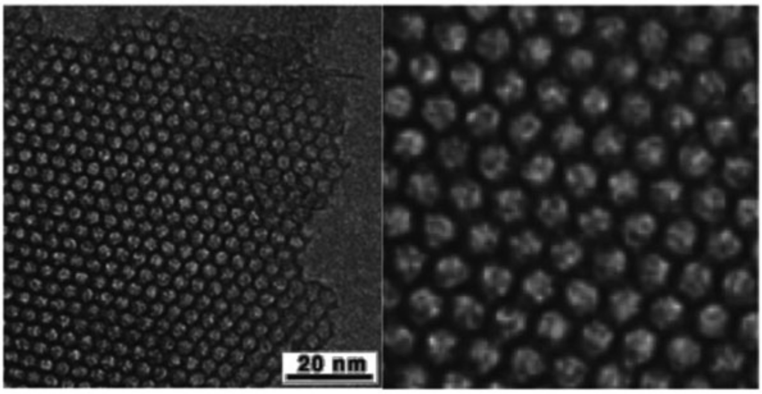

Figure 3. TEM image of an MCM-41 material with a pore size just over 4 nm. The image on the right is an expanded view of a portion of the image on the left. (Adapted from Kruk *et al.* [174], Copyright (2000) American Chemical Society).

materials have also been applied in biotechnology as bioadsorbents and biocatalysts [5], and as drug delivery vehicles [16,17]. These materials differ from zeolites in that the atomic-level structure is amorphous rather than crystalline. The ordering occurs at longer length scales and is created by cooperative templating using surfactants or block copolymers. Figure 3 shows a TEM image of an MCM-41 material [15,18]. This material consists of banks of cylindrical pores in a hexagonal array. The pore sizes can be varied between about 2 and 20 nm depending on the structure of the surfactant. The walls of the pores are amorphous silica. Note that the pore size and the length scale of the ordering are an order of magnitude greater than for the zeolite framework shown in Figure 1. Tremendous effort has been made to understand the formation mechanism of these materials and to develop new materials with advanced functionalities [1,2,15,19–29].

Just as in the case of zeolites, making new ordered mesoporous materials has been accomplished primarily through trial-and-error experimentation, the amorphous atomic structure and detailed formation mechanism of MCM-41 remain poorly understood [15]. Molecular modelling has the potential to provide microscopic insights into these issues, and may offer design principles for controlling pore size, wall structure, surface morphology and defects in mesoporous silica materials.

A central theme of this article, and consistent perspective taken by its authors, is that the syntheses of these types of materials – zeolites and ordered mesoporous materials, as well as other related nanoporous silica materials – can be understood within a single modelling scheme: the modelling of silica polymerisation in the presence of different types of ‘structure-directing’ agents (SDAs, also known as a ‘templates’).

Both zeolites and mesoporous silica materials are typically fabricated using the templated sol–gel synthesis route, involving a silica source, an alumina source when making aluminosilicates, aqueous solvent, acid or base to tune silica solubility and polymerisation kinetics and an SDA to induce, in some way, the formation of porous structures [30]. Standard templates include the organocations tetra-propyl-ammonium (TPA) for synthesising the all-silica zeolite silicalite, and cetyl-trimethyl-ammonium (CTA) surfactants for making MCM-41. Although mechanistic understanding of zeolite nucleation and growth remains incomplete, there is considerable evidence that critical nuclei fall into the 5–10 nm range for both all-silica [31–33] and aluminosilicate zeolite materials [34–36]. Determining structures of such zeolite critical nuclei remains one of the holy grails of zeolite science.

Elucidating the mechanisms by which ordered nanoporous materials form has remained challenging for experiment and theory alike, experiments with atomic resolution suffer from a nanoscale blindspot at length scales where zeolite nucleation is likely to occur [37]. Indeed, NMR provides distances and chemical environments within 1–2 nm, while XRD probes crystalline structure for solids with long-range order above 50 nm. It is in this intermediate length scale range that molecular modelling offers great promise for elucidating zeolite nucleation [38]. However, such modelling still remains a daunting task, requiring relatively long length and timescales on the molecular level; a mix of physical interactions such as electrolytic, hydrophobic and solvation effects; chemical interactions such as silica polymerisation; and efficient sampling of potentially glassy systems. It is, thus, clear why this problem has remained a grand challenge for several decades. However, the field is now poised to make major inroads into the problem of understanding zeolite nucleation through the approaches reviewed in this article.

1.2. *A modelling perspective*

In developing a modelling approach to silica nanoporous materials formation, it is important to reflect on the key structural features of four-coordinate silica polymorphs that are central to understanding their properties, whether we are considering the naturally occurring denser polymorphs of four-coordinate silica such as quartz or cristobalite or all-silica zeolite frameworks such MFI and SOD. Also, we might ask what it is that gives rise to such a large variety of structures of silica.

Table 1. Cohesive energies of silica polymorphs in eV/SiO_2 relative to alpha-quartz from DFT in the local density approximation. Experimental values are shown for some cases. (Adapted from Astala *et al.* [39]).

Structure	DFT-LDA	Experiment
α-Quartz	0	
β-Quartz	0.02	
α-Cristobalite	0.03	0.029 [40]
β-Cristobalite	0.03	
β-Tridymite	0.04	
Sodalite	0.05	
Chabazite	0.07	0.118 ± 0.016 [100]
Mordenite	0.05	
LTA	0.08	
Silicalite (MFI)	0.05	0.070 ± 0.008 [100]

A significant insight emerges from considering the binding energies of various silica polymorphs [39]. Table 1 shows these binding energies relative to that of alpha-quartz (20 eV per SiO_2 unit) as calculated from density functional theory (DFT) together with some measured values from drop calorimetry experiments [40,41]. What we see is that the energy differences, while not zero, are much smaller than the binding energy of α-quartz. This result suggests the following base case picture of the silica energy landscape: a very large number of energy minima with similar energies and with the barriers between them determined primarily by the topology of the network of corner-sharing tetrahedra. (There are some exceptions to this, e.g. quartz, cristobalite and tridymite, where the transformations between α and β forms are displacive, i.e. they do not require breaking and reforming of the network). To illustrate our point of view about of silica structures, Figure 4 shows four silica polymorphs and the role of

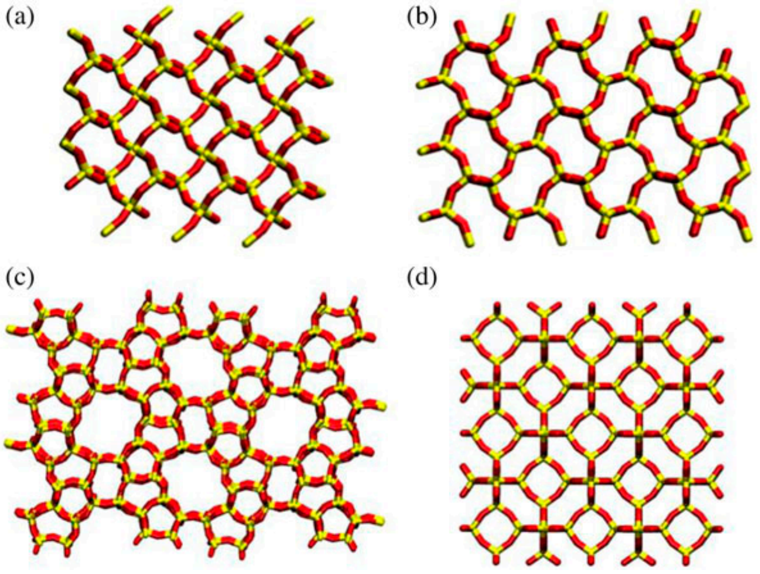

Figure 4. (Colour online) Visualisations of four silica polymorphs. (a) alpha-quartz, (b) alpha-cristobalite, (c) MFI and (d) SOD.

corner-sharing tetrahedral in the structures is evident. It is not difficult to appreciate that there must be an extremely large number of possible silica polymorphs arising from the very large number of ways of arranging corner-sharing tetrahedra into network structures, especially considering the floppiness of the Si–O–Si bond angle. For aluminosilicates, the numbers are even larger. The Atlas of Zeolite structures [10] lists over 200 zeolite structures that have been synthesised and characterised. Moreover, the remarkable databases of hypothetical zeolite structures prepared by the groups of Foster and Treacy [42] and of Deem [43,44] list candidate structures numbering in millions. Synthesis methods for zeolites can be thought of as navigating the complex energy or free energy landscapes of silica or aluminosilicates without negotiating the connectivity barriers between different polymorphs. This is achieved through silica or aluminosilica polymerisation in the presence of structure directing agents. This is similarly true for mesoporous silica materials.

The synthesis of mesoporous silicas involves polymerisation of silica in the presence of surfactant or block copolymer SDAs. These materials exhibit order on the length scale of nanometers or tens of nanometers, but are non-crystalline on atomic length scales in contrast to the atomic scale crystalline ordering in zeolite frameworks. Thus, they are not silica polymorphs in the traditional sense, because of the presence of terminal SiOH groups. In the first instance, the range of structures comes from the range of possible mesophases in the solvent–silica–surfactant phase diagram, with the pore sizes determined by the sizes of the groups in the surfactant or block copolymer. The range of possible structures can be expanded by introducing hierarchical ordering leading to ordered structures with multiple pore sizes. Such hierarchical order can be achieved in several ways, including the use of mixtures of SDAs of different sizes, [45–47] multifunctional SDAs that can produce order on different length scales [48] and templating approaches such as those used to make the three dimensionally ordered mesoporous imprinted (3DOm-i) silica materials [49]. In some cases, these materials combine mesoporosity with microporosity, which may even be in the form of local zeolite framework structuring.

In later sections of this article, we will review several modelling approaches to silica self-assembly. However, we have a preference for approaches that focus on the assembly of tetrahedral units and do not allow the breakage of these units. In part, this preference is based on the need to reduce complexity if we are to study silica polymerisation at sufficiently long length scales required for modelling porous material assembly. But the structure and stability of silica polymorphs clearly guides us towards this approach. Moreover, it provides the basis for a modelling approach that can, in principle, describe the synthesis of all nanoporous silica materials. The approach was inspired by previous work by Dove and co-workers in understanding the properties of silica materials as assemblies of rigid units [50,51].

1.3. *Outline of article*

The remainder of this review is organised as follows: in Section 2, we outline the current thinking in how amorphous silica, zeolites and mesoporous materials form; in Section 3, we detail recent quantum calculations on silica condensation chemistry; in Section 4, we review recent simulations on silica-SDA interactions; in Section 5, we describe recent breakthroughs in our ability to model silica polymerisation and nanopore crystal formation; in Section 6, we review recent breakthroughs on modelling mesoporous material formation; and in Section 7, we offer a summary and outlook on the field of modelling ordered nanoporous silica.

2. Survey of synthetic methods and mechanistic understanding

Experimental understanding of the formation mechanism of amorphous silica, mesoporous silica and crystalline zeolites has been investigated for decades. The formation process usually includes the formation of silicate species, polymerisation of the silicate species and their assembly to form mesoporous structure or crystalline microporous structure in the presence of amphiphilic molecules, organic amines or inorganic cations as SDAs [30,52].

2.1. *Formation of amorphous silica*

Amorphous silica is usually synthesised by a sol–gel process [53,54]. The process involves the hydrolysis and condensation of silicon alkoxide such as tetraethylorthosilicate (TEOS) and tetramethylorthosilicate (TMOS) in a mixture of water and alcohol. The reactions of silicon alkoxide into amorphous silica by the sol–gel process can be written as:

$$\text{Hydrolysis}: \quad \mathrm{Si(OR)_4 + H_2O \rightarrow Si(OH)_4 + 4ROH}$$

$$\text{Condensation}: \quad \mathrm{2Si(OH)_4 \rightarrow (OH)_3Si - O - Si(OH)_3 + H_2O.}$$

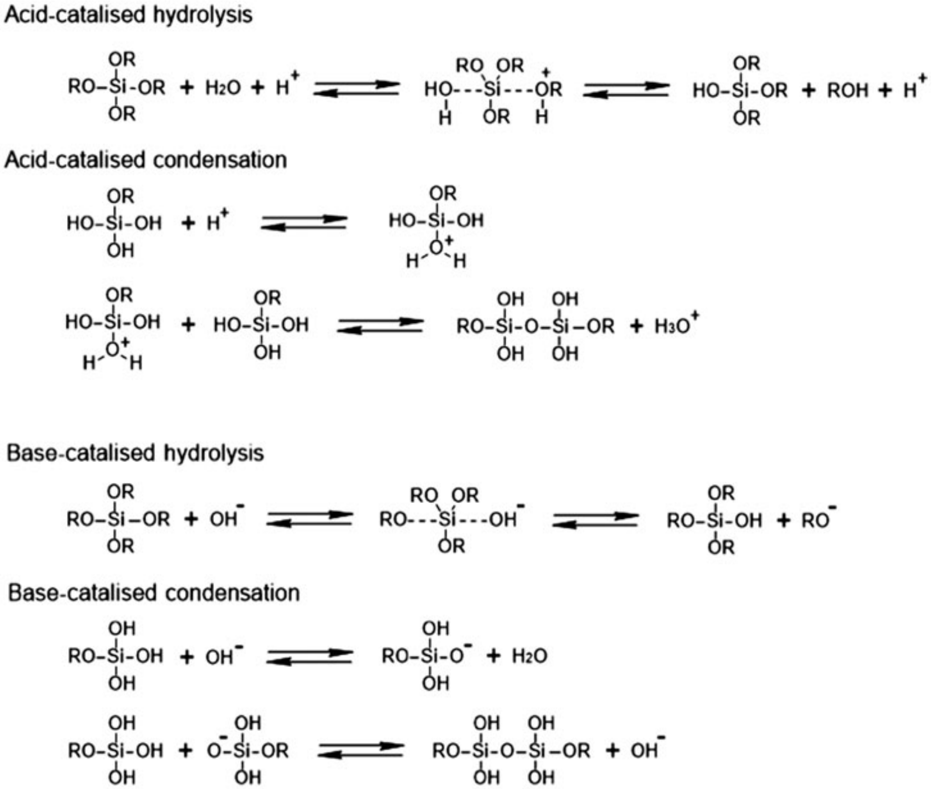

Figure 5. Hydrolysis and condensation mechanism for the synthesis of amorphous silica under acidic and basic conditions, respectively.

The hydrolysis of silicon alkoxide leads to the formation of silanol groups that can react with each other to create siloxane bridges (Si–O–Si). Extended silica structures are formed by a series of condensation reactions between monomers and oligomers. It has been known that the hydrolysis and condensation reactions can be catalysed by either an acid (e.g. HCl) or a base (e.g. NH_3) [53–55].

As shown in Figure 5, the acid-catalysed hydrolysis is performed by the rapid protonation of –OR in the first step [55,56]. Electron density is withdrawn from silicon, making it more electrophilic and susceptible to be attacked by water. It is generally believed that the hydrolysis occurs by bimolecular nucleophilic displacement reactions [54,55]. Under acid conditions, silica tends to form linear polymeric chains that can be occasionally further cross-linked [53,54,56]. Base-catalysed condensation involves the nucleophilic attack of a deprotonated silanol group on a neutral silicate specie [53–56]. The hydrolysis and condensation reactions under basic conditions usually produce highly branched clusters, eventually leading to the formation of three-dimensional amorphous silica structure [53,54,56]. It remains to be seen whether molecular modelling can reproduce the qualitative distinction between acid-catalysed silica chains and base-catalysed 3D silica networks observed experimentally.

Structural evolution of silicate species into amorphous silica particles has been studied using various experimental techniques such as NMR, small angle X-ray scattering (SAXS) and infrared and Raman spectroscopy. In the early stage of hydrolysis and condensation of TEOS, aqueous silicate species including three monomer species ($Si(OH)_4$, $SiO(OH)_3^-$ and at sufficiently high pH, $SiO_2(OH)_2^{2-}$) and several oligomeric species were observed by ^{29}Si NMR [57,58]. Engelhardt *et al.* reported that condensation sequence is commonly monomer, dimer, trimer, cyclic trimer, cyclic tetramer and higher order ring structures [59]. In addition, a SAXS measurement on the condensation process suggested that the silicate oligomers formed under acid conditions (e.g. pH 1.0) are more condensed than the one formed by base-catalysed reactions [60,61]. Amorphous silica particles can be formed by the assembly of the silicate oligomers formed in the initial stage of the growth process.

Two main models have been developed for the growth process based on experimental findings. They are monomer addition growth proposed by Matsoukas and Gulari [62–64], and controlled aggregation growth proposed by Zukoski and coworkers [54,65–67]. In the monomer addition model [62–64], the formation of silica particle starts with the reaction between two silicate monomers, and particles can grow only by monomer addition. This model requires a continuous source of monomers for particle growth. The final particle size and particle size distribution are determined from the balance between nucleation and monomer addition. The particle growth process has been found to be reaction limited by the hydrolysis of the monomer. In particular, Matsoukas and Gulari reported that the first-order rate constant of hydrolysis was identical to the time constant for the silica particle growth, supporting that this growth is limited by the hydrolysis reaction [64]. Blaaderen *et al.* also showed that the overall rate of the particle growth is limited by the first-order hydrolysis rate of the alkoxide, established using ^{13}C NMR and the time-resolved static light scattering [68].

On the other hand, according to the controlled aggregation growth model proposed by Zukoski and colleagues [54,65,66], there is a continuous generation of primary particles of several nanometers in size that are further aggregated during particle growth. In this model, the final particle size and its distribution are influenced by parameters such as the surface charge and the size of the primary particles. A study of the particle growth performed by transmission electron microscopy (TEM) revealed that tiny particles coalesce to form primary particles [66,67]. Experimental study has not provided a complete description on the nucleation of amorphous silica particles. It is believed that the formation mechanism is strongly influenced by the silica source and pH value. Further experimental and computational studies on the nucleation process and amorphous structure of the formed silica particles are needed.

2.2. *Formation of mesoporous silica through co-assembly with surfactant*

Mesoporous silica materials are synthesised by the polymerisation of silicate species in the presence of surfactants. Highly ordered and tunable mesoporous structures with a pore size from 2 to 20 nm and structure from 1D to 3D can be achieved using different surfactants and controlling the polymerisation kinetics of the silicate species. Different from zeolites and other microporous crystalline materials, mesoporous silica exhibits an amorphous silica structure in its wall similar to silica particles. Based on experimental studies, cooperative self-assembly and true liquid crystal templating mechanisms have been proposed for the assembly and formation of silica-based mesostructured materials [2,69–71]. In the true liquid crystal templating mechanism, the surfactant concentration is high, and the surfactant molecules arrange into specific liquid-crystalline phase under given reaction conditions. The formed liquid crystals then serve as templates for the formation of mesopore structure. Attard *et al.* used liquid crystalline phases of the non-ionic surfactants (octaethylene glycol monododecyl ether ($C_{12}EO_8$) and octaethylene glycol monohexadecyl ether ($C_{16}EO_8$)) as a template to synthesise mesoporous silica. It was observed that the resulting silica phase from the template is an exact replica of the surfactant mesophase [72]. Mesoporous silica with hexagonal, cubic and lamellar symmetries can be readily obtained by the approach.

The cooperative self-assembly mechanism involves the development of self-assembled liquid crystal micelles composed of both inorganic species (e.g. silica source) and surfactant molecules at a surfactant concentration lower than the critical micelle concentration. Based on a series of experimental studies, Huo *et al.* proposed that the driving force for the formation of micelle structure is the attractive interaction between the surfactants and inorganic species [73]. The assembly process is governed by charge matching at the interface of the inorganic/organic phases. The formation of MCM-41, an important mesoporous silica material with highly ordered hexagonal array of pores, is a grand example of this pathway. In this case, the silicate species interact with the positively charged head groups of the cationic surfactants (CTA^+, cetyl trimethylammonium) followed by polymerisation in the interface region. Davis *et al.* have shown that the liquid crystalline phase does not exist in the synthesis medium during the formation of MCM-41 using *in situ* ^{14}N NMR. This result supports the cooperative self-assembly pathway [21]. Besides cationic surfactant (S^+) and anionic inorganic species (I^-) combination, it has been also proposed that using anionic surfactant cooperative with cationic inorganic species (S^-I^+) can also form ordered mesoporous inorganic phases. Moreover, by incorporating counter ions with opposite charge of both surfactant group and inorganic specie ($S^+X^-I^+$ and $S^-M^+I^-$, where $X^- = Cl^-$, Br^- and $M^+ = Na^+$, K^+), the formation of mesoporous structure has also been observed [73]. These pathways are mainly dominated by electrostatic forces. Moreover, the cooperative formation mechanism can also be found in a non-ionic surfactant system (S^0), such as SBA-15, synthesised in a highly acidic condition with a triblock copolymer (P123, PEO-PPO-PEO), likely via a double-layer hydrogen bonding interaction ($S^0H^-X^-I^+$) [74]. S^0I^0 and N^0I^0 (neutral amines) systems are also present through hydrogen bonding interaction, and disordered mesoporous silicates were obtained [75,76]. As discussed below in Section 6, a major challenge in developing more complete understanding of the cooperative self-assembly mechanism is determining whether silica monomers or a range of oligomers participate with surfactants in the generation of mesoscale order.

The amorphous structure of silica particles and mesoporous silica largely limits their applications in catalysis and separation because of the lack of molecular sieving property and low hydrothermal stability. Crystallisation of the amorphous structure of mesoporous silica and recent breakthrough in the synthesis of mesoporous zeolites provide exciting opportunities for developing the porous materials with new structures and functions.

2.3. *Formation of microporous crystalline materials*

The crystallisation mechanisms of zeolites under hydrothermal conditions have been experimentally studied for decades. The formation of nuclei and the subsequent crystal growth are not yet fully understood even for the most well-studied zeolites (e.g. MFI zeolite), which are mainly due to the lack of characterisation techniques capable of *in situ* monitoring of structure evolution, and the challenge in the understanding and modelling the thermodynamics and kinetics of the crystallisation process, as discussed further below. Here, we summarise the experimental results of the zeolite crystallisation process including the interaction between the SDAs and silicate species, the formation of amorphous particles and the evolution of structure from disorder to order. Following it, we will discuss the parameters affecting the thermodynamics and kinetics of zeolite formation sampled by experimental studies.

In 1959, Barrer *et al.* first discussed the synthesis mechanism of aluminosilicate zeolites made in the presence of inorganic cations [77]. They speculated that the crystallisation process involves the formation of ring structures of tetrahedra or polyhedral that can be 3–6 tetrahedra, double 4-rings and double 6-rings. Following the pioneering work of Barrer in the synthesis of zeolites, Breck and Flanigen used XRD and microscope to study the crystallisation processes of zeolites and proposed important information for the nucleation and crystal growth of zeolites [78]. It was proposed that the nuclei do not necessarily represent a unit cell, but may consist of more preliminary building units of polyhedra; and the growth of crystal proceeds through a type of polymerisation and depolymerisation process catalysed by excess hydroxyl ion, and involves both the solid and liquid phases. Breck also suggested that the hydrated cations could direct the formation of basic polyhedral units and subsequent assembly of ordered crystal structure of zeolites. Whether or not the nucleation of zeolites occurs in the gel or solution phase has been discussed by Kerr and Ciric [79–81], they both highlighted the importance of a solution-mediated growth mechanism that involves the dissolution of the amorphous gel and the transport of growth species to nuclei from the solution phase.

Since the 1960s, organic SDAs (OSDAs) were used in zeolite syntheses. The use of tetramethylammonium (TMA) led to the formation of zeolite A with a higher Si/Al ratio [79,82,83]. First, high silica zeolite Beta was synthesised in the presence of tetraethylammonium (TEA) cation [84]. After that, ZSM-5 with a MFI structure was synthesised using TPA, and led to a revolution in the use of zeolite catalysts for oil refining [85]. The use of OSDAs in zeolite synthesis opened an important new avenue for the development of zeolite structures and compositions. Most new zeolite structures discovered in the past four decades have involved the use of OSDAs [86–88]. The crystallisation mechanism of zeolites in the presence of OSDAs is clearly different from the ones proposed previously for the zeolites synthesised in alkaline solutions. Extensive efforts have been devoted to understanding the interaction between OSDAs and silicate species, and subsequent nucleation and growth processes.

Chang and Bell systemically studied the crystallisation process of silicalite-1 (MFI structure) in the presence of TPA using XRD and ^{29}Si NMR. They proposed that the OSDA can form clathrate-like water structures and subsequently form clathrate-like silicates by isomorphous substitution of silicate for water [89]. The concept was developed in detail by Davis using a series of ^{1}H–^{29}Si CP MAS NMR measurements [90,91]. The NMR study provided direct evidence for the presence of inorganic-organic composite structures. It is believed that composites are formed by the overlap of the hydrophobic hydration spheres of the inorganic and organic components. The release of ordered water molecules from the overlap enables favourable van der Waals interactions and an entropy-driven assembly process. Nucleation is, then, proposed to occur through aggregation of these composite species, followed by crystal growth through diffusion of the composite species onto the surface of growing crystallites, leading to a layer-by-layer growth mechanism as shown in Figure 6. *In situ* characterisation studies using small angle SAXS and cryo-electron microscopy have further elucidated the nucleation and crystal growth of silicalite-1 in the presence of TPA, and revealed that the crystallisation is driven by the evolution of the precursors (from 2 to 10 nm) formed in the initial stage of the synthesis [90,91].

More recent studies reported that the formation of precursor particles with a size of around 5 nm is critical for the nucleation and growth of zeolites. The structure and composition of the precursor particles remains unclear. The recent reports from Vlachos and Lobo *et al.* suggested the precursor particles formed a core–shell structure with

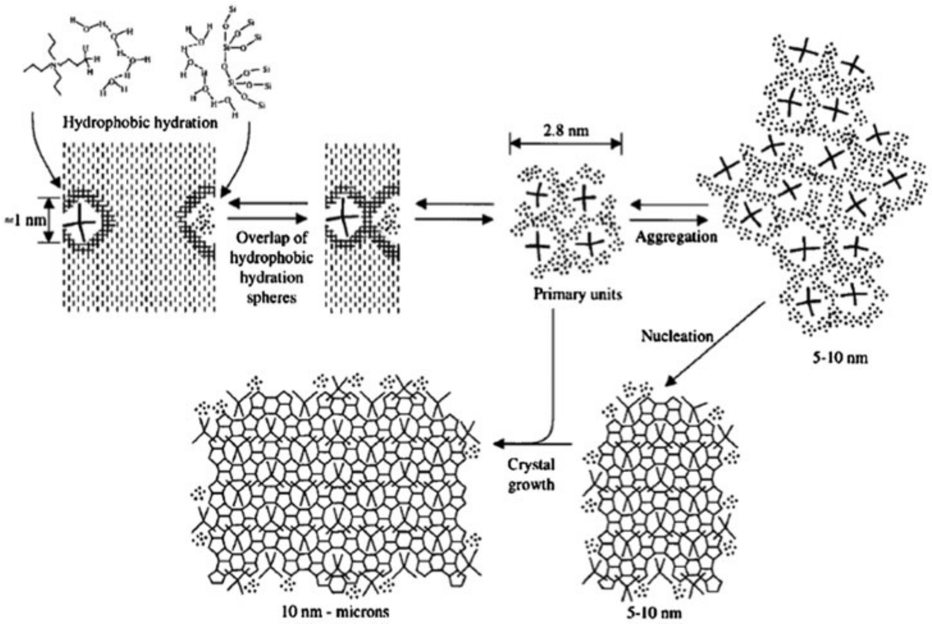

Figure 6. Scheme for crystallisation mechanism of silicalite-1(MFI) in the presence of TPA. Reprinted with permission from de Moor *et al.* [91]. Copyright (1999) Wiley-VCH Verlag GmbH, Weinheim, Fed. Rep. of Germany).

OSDA rich in the shell [92]. Tsapatsis *et al.* also suggested that the precursor nanoparticles evolve to zeolite crystals through several intermediate states that can contribute to an aggregative growth [31,32,37,93,94]. A long-range order, corresponding to a zeolite crystalline phase, was observed in the particles with a size of around 10 nm composed of the precursor particles having a size of around 3 nm. The precursor particles also participated in crystal growth. Tsapatsis and Vlachos *et al.* reported that the van der Waals attraction and electrostatic repulsion might be used to describe the interaction between zeolite seeds and precursor particles [95]. A similar crystallisation scheme has been proposed for several other conventional zeolites including zeolite LTA, FAU, and BEA [35,36,96–98].

Fundamental understanding of zeolite crystallisation requires knowledge of the interplay between the thermodynamics and kinetics of zeolite nucleation and growth. Here, we summarise key experimental aspects of both topics prior to a detailed description of the state-of-the-art theoretical studies on the zeolite crystallisation mechanism. Using calorimetry technique, Navrotsky and coworkers have thoroughly studied the critical parameters influencing the thermodynamics of zeolite synthesis, which includes framework density, composition (Si/Al), extra framework cation and hydration [99–101]. A positive correlation between the molar volume of high-silica zeolite frameworks and the heat of formation of zeolite (denoted as relative heat of formation, $\Delta H^0_{f,zeolite} - \Delta H^0_{f,quartz}$) was found (Figure 7), indicating that zeolites with open frameworks exhibit less favourable enthalpies of formation compared with the dense zeolites and quartz. Navrotsky also reported that introducing Al into the framework is more thermodynamically favourable for zeolite formation, which is also closely related with the type of extra framework cations [101]. It should be also noted that most of the calorimetry measurements were carried out with anhydrous zeolites. For the zeolites grown from an aqueous phase, the effects of hydration on the thermodynamics of zeolite formation must be considered. It has been known that several factors can affect the hydration of zeolites [102]. High silica zeolites are hydrophobic and adsorb less water than do low silica zeolites. The hydration state of extra framework cations and

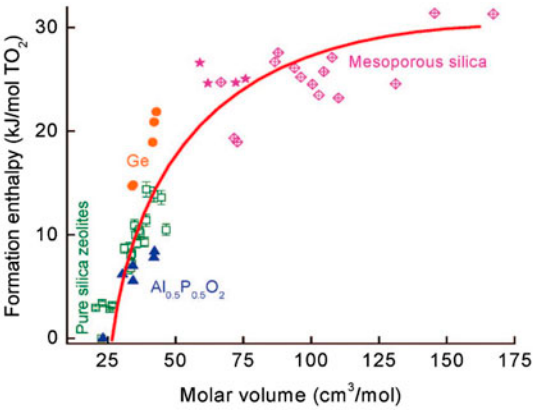

Figure 7. (Colour online) Formation enthalpies for silica zeolites, Ge and Al phosphate zeotypes and mesoporous silica: green symbols, dense and zeolitic silica phases; blue symbols, aluminophosphates; orange symbols, Ge-zeolites; magenta symbols, mesoporous silica cubic (stars) and hexagonal (diamonds). (Reprinted with permission from Navrotsky *et al.* [101]. Copyright (2009) American Chemical Society).

the number defects can also affect the overall thermodynamics of the zeolite formation. Due to the complexity of zeolite formation processes and a large of number of factors as well as the accuracy of experimentally measured heat of formation, it is still a grand challenge to make a full thermodynamic description of zeolite formation based on experimental measurements.

Based on the thermodynamics of zeolite formation with different structures and compositions, the Ostwald step rule has been used to describe nucleation and phase transition in natural and synthetic zeolite crystallisation [103]. The fundamental principle of the Ostwald step rule is the evolution of structure with time, including the initial formation of a metastable phase and subsequent transformation through a series of stages to more thermodynamically stable structures. The different Ostwald steps can be a distinct crystal structure change or less distinctive such as from amorphous to crystalline transition. Navrotsky has reported that the heat of formation for siliceous zeolites fall within 6.8–14.4 kJ/mol above quartz [101]. The narrow range of the heat of formation for the zeolites with different structures motivates our unique modelling perspective discussed above in Section 1.2, and highlights that the kinetic factors might play critical roles in the structures of formed zeolites. In addition to siliceous zeolites, different heteroatoms (e.g. Al, Ge, P, etc.), extra framework cations and hydration can also largely affect the heat of formation of stable zeolite phase. Unfortunately, quantitative information of the heat of formation of zeolite with the variables is not available for most zeolite structures. Predicting stable zeolite phases, thus, requires comprehensive understanding of the effects of each factor on the thermodynamics of zeolite crystallisation, which is currently unattainable from experimental study.

Previous studies have suggested that the initial formation of amorphous particles as a metastable phase seems to be indispensable in the zeolite formation process [104]. The physicochemical factors for zeolite nucleation from the amorphous phase to crystalline nuclei are not fully understood, but seemingly occur through several stages involving the structural rearrangement in the initially formed precursors and dissolution/recrystallisation processes. The formation of amorphous precursors and evolution of the amorphous structure to crystalline forms have been extensively observed for siliceous MFI zeolites (Silicalite-1). Both high resolution TEM images and small angle X-ray/neutron scattering studies have indicated a disorder-to-order transition, which could be explained by structure rearrangement in the amorphous particles and/or dissolution/recrystallisation from liquid phase [37,95,98,105]. High resolution TEM images have also revealed the formation of nuclei in the amorphous particles for LTA and FAU formation, seemingly followed by the dissolution of the residual part of the amorphous particles [106,107].

Due to the relatively minor difference in the heat of formation of various zeolites, kinetic parameters including the dissolution of the initial formed amorphous particles, rearrangement and evolution of the structure in the amorphous particles, the growth the formed nuclei must be investigated. Understanding of zeolite crystallisation mechanism require the ability of coupling the thermodynamics and kinetics parameters in the synthesis process (e.g. composition, pH, structure directing agent, temperature …), which is not been fully achieved by experimental studies yet.

3. Quantum chemistry of the thermodynamics and kinetics of silica condensation

Catlow and coworkers have reported several studies employing quantum chemistry and molecular simulations to investigate key species thought to participate in the formation of zeolites, with a focus on energetics of stable species for computational efficiency. This emphasis is consistent with the assumption of thermodynamic control in zeolite synthesis. Their initial study, reported in two parts in 1999 by Pereira *et al.* applied DFT to investigate the energetics of relatively simple [108] and more complex [109] gas-phase silica oligomeric species. The study of relatively simple silica species (monomers up to pentamers and the cubic eight-silicon cage) showed no simple trend in energy or charge distribution [108]. The study on more complex structures (e.g. branched and ring structures) showed that the stability of the non-cyclic clusters decreases with the degree of branching, that double-ring clusters are quite unstable, and that four- and six-silicon rings (i.e. rings with four or six alternating units of –(Si–O)– atoms, henceforth denoted 4- and 6-rings) are more stable than the corresponding 5-ring, presumably because of the relatively asymmetric arrangement of the 5-ring silica species [109].

A more recent study in 2012 by Yang *et al.* applying DFT with solvent corrections using the continuum 'COSMO' approach, investigated the thermochemistry of the polymerisation of aluminosilicate clusters [110]. The major finding in this work is that the participation of $NaAl(OH)_4$ species in condensation reactions is unlikely as this would result in zeolites in violation of Löwenstein's rule, which forbids adjacent AlO_4 tetrahedra in zeolites, and hence forbids zeolite Si/Al ratios less than unity, presumably because of electrostatic repulsion between negative centres. This work suggests, instead, that growth may occur predominantly via the $NaAlSiO(OH)_6$ dimer.

Most recently, in 2013, Yang *et al.* reported DFT calculations of the Gibbs free energies of various species thought to play roles in the formation of the cubic zeolite NaA [13]. They applied the COSMO continuum solvation method to estimate solvent effects, and assumed ideal gas/rigid rotor/harmonic oscillator statistical mechanics to compute enthalpies and entropies of the various species considered. The structure of zeolite NaA features double 4-rings connecting so-called sodalite (cubo-octahedral) cages [10], prompting the authors to compute energies for species involving such 4-rings. Their results suggest that 4-ring species may, indeed, be the most likely to participate in the nucleation of zeolite A, and its nucleation mechanism could proceed by a reaction that involves the formation of the double 4-ring. Advanced characterisation methods such as ^{29}Si NMR are required to test the predictions of these groundbreaking calculations.

Van Santen and coworkers have also reported several studies on the physical chemistry of silica polymerisation, with a focus on the *kinetics* of silica condensation. To put their focus on kinetics into perspective, we note, as discussed above, that the formation of zeolites is presumed to be controlled by kinetics – a conclusion based on both computational energetics and experimental syntheses. Regarding energetics, quantum calculations on all-silica zeolites produce energies that are consistently higher than that of α-quartz [39], the thermodynamically stable state of SiO_2 at low temperatures and pressures such as STP. This suggests that all-silica zeolites become trapped in metastable states during synthesis and/or post-synthetic treatment (calcination and drying). Regarding experimental syntheses, several zeolite preparations are known to pass through several different zeolite phases as a function of synthesis time [111–114], a key signature of kinetic control. As such, investigations into the microscopic kinetics of silica condensation and polymerisation may shed important light on zeolite formation.

In 2006, Trinh *et al.* reported the application of DFT including solvent corrections with COSMO to compute pathways and transition states for neutral/neutral [$2Si(OH)_4 <=> (OH)_3Si–O–Si(OH)_3 + H_2O$] and anionic/neutral [$Si(OH)_4 + SiO(OH)_3^- <=> (OH)_3Si–O–SiO(OH)_2^- + H_2O$] silica condensation processes [115]. As shown below in

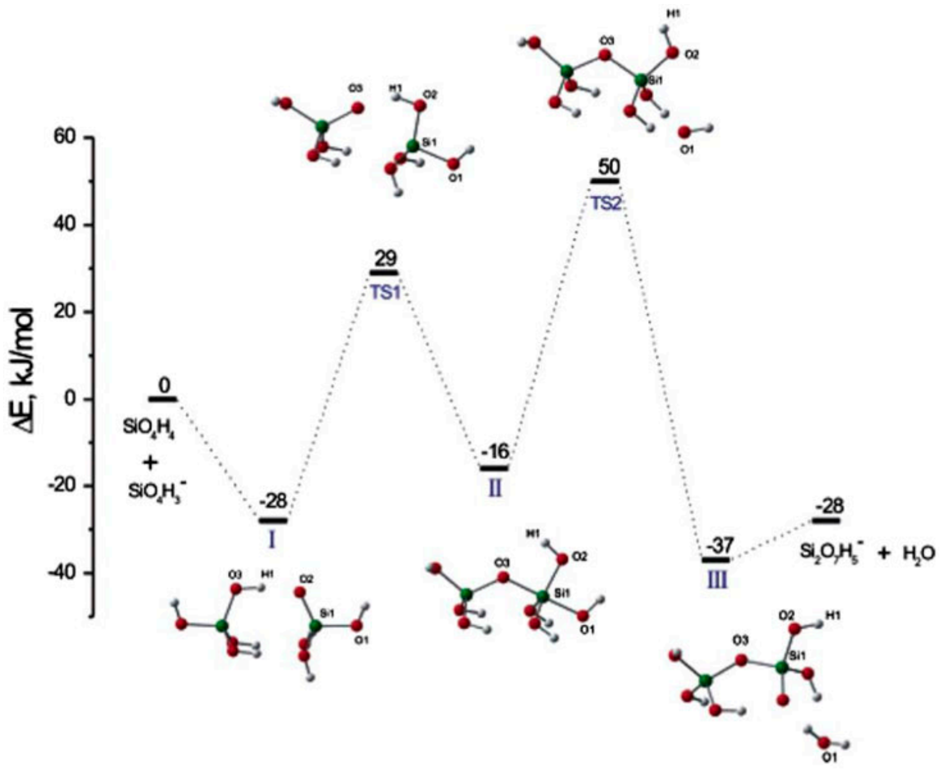

Figure 8. (Colour online) Microkinetic pathway and energetics for anionic/neutral silica condensation (B3LYP/6–31 + G(d,p) – COSMO). (Reprinted with permission from Trinh *et al.* [115] Copyright (2006) American Chemical Society).

Figures 8 and 9, Trinh *et al.* found that the anionic/neutral process is *strongly* favoured kinetically over the neutral/neutral condensation. The neutral/neutral process was found to be direct (with only a single transition state, see Figure 9), while the anionic/neutral condensation is a two-step process with an intermediate (after forming the bridging oxygen, but prior to releasing water, see Figure 8) involving silicon in a pentavalent, trigonal-bipyramidal structure. The electron-rich nature of the anionic complex likely stabilises this relatively rare pentavalent silicon [116], thus making the anionic/neutral condensation kinetically favoured.

An analysis of the energetics in Figures 8 and 9 leads to interesting conclusions. First, both the anionic/neutral and neutral/neutral condensations are equally exothermic (by about –10 kJ/mol) from interacting reactants to interacting products. This shows a lack of correlation between the reaction and activation energies for these two processes, further warranting the need for kinetic studies of silica condensation. Second, for both anionic/neutral and neutral/neutral processes at the B3LYP/COSMO level of theory, there is an endothermic process (by + 9 and + 17 kJ/mol, respectively) of $(\text{dimer–water})_{aq} \rightarrow (\text{dimer})_{aq} + (\text{water})_{aq}$. Clearly, if COSMO provided a perfectly accurate treatment of aqueous solvation (aq), the energy change for both processes would vanish. As such, the 9–17 kJ/mol energy change provides an estimate of COSMO's error in hydration energies. This order of magnitude in hydration energy error is *much* smaller than the difference between the barriers for anionic/neutral and neutral/neutral

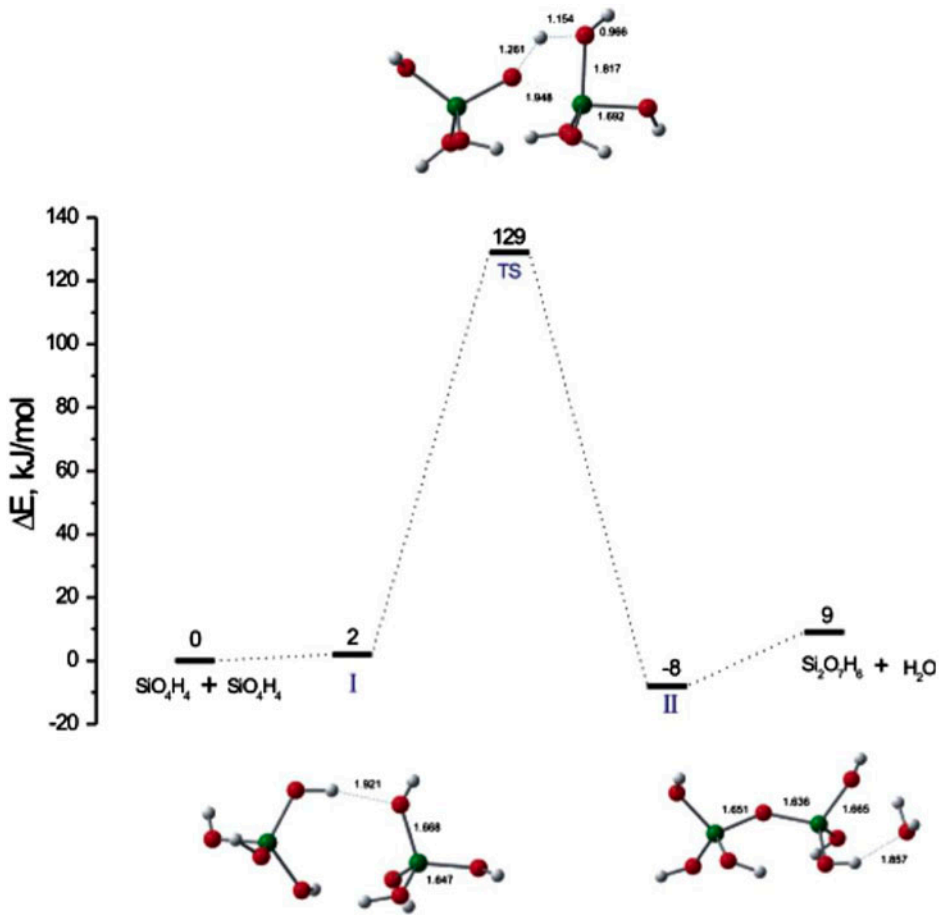

Figure 9. (Colour online) Microkinetic pathway and energetics for neutral/neutral silica condensation (B3LYP/6–31 + G(d,p) – COSMO). (Reprinted with permission from Trinh *et al.* [115] Copyright (2006) American Chemical Society).

processes (anionic/neutral barriers: 57 and 66 kJ/mol; neutral/neutral: 127 kJ/mol, respectively), suggesting that the kinetic favorability of the anionic/neutral process remains a robust conclusion even with error in computing hydration energies. However, the presence of this hydration energy error prompted Van Santen and coworkers to pursue more accurate treatments of hydration in subsequent work.

In 2009, Trinh *et al.* reported *ab initio* molecular dynamics (AIMD) calculations of the kinetics of the anionic/neutral condensation using explicit aqueous solvation with the Car-Parrinello (CPMD) code and the BLYP density functional (see Figure 8) [117,118]. We note that BLYP provides an approximate treatment of identical fermion exchange as compared with the exact treatment of exchange in B3LYP; as a consequence, BLYP reaction barriers are typically lower than those from B3LYP. Trinh *et al.* found that changing from a continuum (COSMO) water model to an explicit treatment of hydration reduces barriers for SiO–Si bond formation (to about 45 kJ/mol), whereas the overall thermodynamics becomes less favourable. In particular, the anionic/neutral condensation reaction energy goes from –9 kJ/mol (COSMO) [115] to +25 kJ/mol (CPMD). It remains unclear how much of these changes can be attributed to the explicit treatment of hydration, and to the approximate treatment of electron exchange in BLYP. It also remains to be seen whether the neutral/neutral condensation process remains exothermic with explicit hydration.

Van Santen and coworkers have also investigated the effects of counter ions on silica condensation kinetics. Trinh *et al.* applied CPMD to study the effects of counter ions Li^+ and NH_4^+ on anionic/neutral silica condensations [119], while Pavlova *et al.* studied the effect of Na^+ on such reactions [120]. They found that these counter ions increase barriers for condensations, because of relatively tight binding to neighbouring waters; hence, decreasing the ability of neighbouring waters to participate in the condensation chemistry. Trinh *et al.* also found that NH_4^+ has little effect on subsequent oligomerisation steps, suggesting that the presence of NH_4^+ kinetically favours the formation of larger silica species.

Despite this progress on understanding silica condensation chemistry, several questions remain. In particular, the dramatic change in the anionic/neutral condensation thermochemistry from thermodynamically favoured [$\Delta E = -10$ kJ/mol for B3LYP/COSMO (implicit water)] to strongly disfavoured [$\Delta E = +25$ kJ/mol for CPMD/BLYP (explicit water)] raises a question about the driving force for silica condensation and eventual polymerisation – why does it happen? More accurate AIMD calculations including explicit water and better treatments of exchange and dispersion interactions are likely needed to answer this question definitively.

4. Molecular simulations of physical interactions in zeolite precursor solutions

Zeolite precursor solutions are rather complex mixtures with aqueous solvent and alcohol co-solvent, organic SDAs, other counter ions such as Na^+, silica sources and oligomers, alumina sources, and eventually zeolite nuclei and crystals. Investigating the physical nature of these solutions, and the precise physical and chemical roles of SDAs, remains important for understanding and eventually controlling zeolite nucleation and growth.

Towards this end, Pereira *et al.* reported molecular dynamics (MD) simulations studying the physical structures of solutions containing alumina and silica growth nutrients necessary for zeolite growth [121]. They applied two different MD codes/forcefields – DISCOVER and DL-POLY – to test for forcefield sensitivity, finding substantially similar results from both forcefields. In particular, they found that silica clusters tended to aggregate in their simulations, even in dilute solutions, which was deemed a necessary step for condensation reactions to occur. This important result indicates that coarse-grained models – e.g. such as lattice models and kinetic Monte Carlo (KMC) models of silica polymerisation and zeolite growth – should contain processes and energetics associated with such aggregation, perhaps driven by a measure of hydrophobicity of neutral silica species in water.

Van Santen and coworkers addressed the question of physical interactions in precursor solutions in several papers starting in 2009, when Szyja *et al.* [122] reported the use of a reactive forcefield to study silica-SDA interactions for structures that lead to the all-silica zeolite silicalite. Szyja *et al.* investigated the behaviour of silicate clusters containing up to 22 Si atoms, interacting with TPA ions, the SDA of choice for making silicalite. They found that TPA cannot be accommodated any more in newly formed silicate cavities, but instead is pushed out to positions where in a later stage, zeolite channel intersections can form. What remains unclear is whether the energetics of the clusters treated by Szyja *et al.* are consistent with the quantum chemistry detailed in the section above. To address this, Verstraelen *et al.* [123] applied static quantum chemistry and MD to study essentially the same questions as Szyja *et al.* finding that when the typical 10-ring channel of silicalite is formed from smaller silica oligomers, TPA is partially excluded from the resulting cavity. Partial retention TPA was, however, found to be important to avoid collapse of the channel. The question remains how *different* SDAs can steer silica polymerisation towards different final zeolite structures.

To address this issue, Szyja *et al.* reported a classical MD study [124] and a quantum chemistry/AIMD report [125] of SDAs interacting with silica species thought to play roles as intermediates in the formation of all-silica zeolites. In particular, they simulated interactions between TPA and silica species believed to be precursors to silicalite (all-silica MFI), and interactions between tetrabutyl ammonium (TBA) and putative precursors to all-silica ZSM-11 (MEL). Szyja *et al.* found that the alkyl chains of TPA and TBA appear to stabilise cavities in silica oligomers, and these SDAs assist in the aggregation of such silica clusters to form channel intersections. In the process, these SDA cations were found to move to locations different from their original positions before aggregation. Szyja *et al.* also reported a possible physical origin for the ability of these SDAs to produce different zeolites [124]. However, it has not been established that the putative silica precursors considered in these studies are indeed intermediates leading to MFI and MEL zeolites. Despite the speculative nature of these studies, they represent important steps toward identifying the physical interactions that determine SDAs direct zeolite formation – one of the grand challenges in zeolite science. The combination of advanced spectroscopic techniques [126] and innovations in molecular modelling will be crucial for identifying precursors that lead to zeolite nucleation, necessary for testing the intriguing predictions of Szyja *et al.* [124,125].

5. Modelling silica polymerisation and zeolite nucleation

With current computer architectures and algorithms, simulating silica polymerisation to experimentally relevant length scales requires the application of more coarse-grained molecular modelling approaches. This limitation of atomic-level modelling arises because of the timescales required for two distinct processes: (i) at shorter length scales, overcoming the substantial condensation barriers discussed above; (ii) at longer length scales, sampling the huge configuration space produced in three-dimensional polymerisation. Experimental characterisation of silica polymerisation is, thus, crucial for testing the validity of coarse-grained modelling methods. Perhaps, the best available test of silica polymerisation models is the so-called Q_n distribution measured by the solid-state ^{29}Si NMR. [127] Q_n is defined as the mole fraction of silicon atoms bound to n bridging oxygens; as such, Q_0 provides the mole fraction of $Si(OH)_4$ monomers; Q_1 counts silica dimers and end groups; Q_2 accounts for silica chains and rings; and Q_3 and Q_4 represent more fully networked silica, culminating in all-Q_4 quartz or crystalline zeolites. The temporal evolution of the Q_n distribution as measured by NMR provides a key target for molecular models to reproduce. Figure 10 compares experiment [127] and Monte Carlo simulation (see below for more details) [128], showing the qualitative evolution of the Q_n distribution in aqueous solution at a pH of 2 – the isoelectric point of silica – at which silica condensation is relatively slow, hence allowing NMR to capture its time evolution.

MD simulations of silica polymerisation using reactive forcefields [129,130] have yet to capture the qualitative evolution of the Q_n distribution, even when the

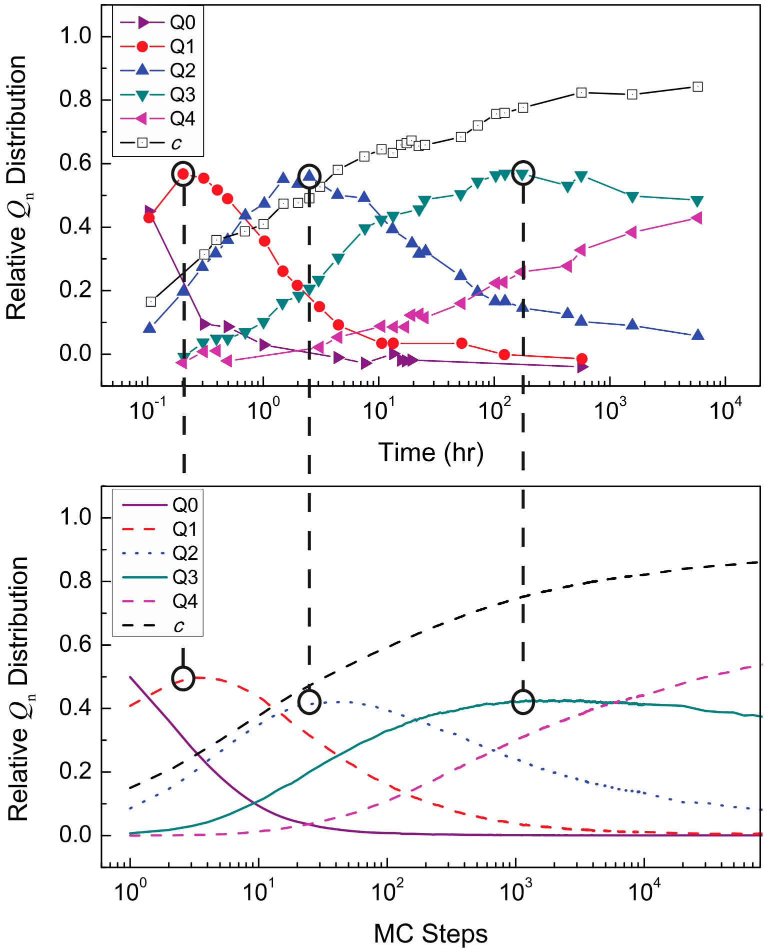

Figure 10. (Colour online) Experiment and Monte Carlo simulation of Q_n distribution. (Reprinted with permission from Jin *et al.* [128] Copyright (2011) AIP Publishing LLC).

simulations are performed at high enough temperatures and silica concentrations to strongly promote condensation processes. We have discussed these MD simulations in our previous review [38], and now turn to more recent Monte Carlo studies that have made substantial progress in our ability to reproduce Q_n distributions.

An initial level of coarse-graining assumes that all-silica polymerisation reactions occur as independent Poisson processes, allowing the application of KMC methods. KMC can *dramatically* extend the timescales that can be sampled, but require all relevant processes to be pre-enumerated and their respective rate constants pre-computed [131]. Such enumeration is often accomplished by assuming lattice models, which convert a continuum of configurations into a countable space, but at the expense of limiting possible structures based on the assumed lattice arrangement. Zhang *et al.* [132,133] modelled the very early stages of silica polymerisation using continuum KMC parameterised by the neutral/neutral and neutral/anionic silica condensation rate constants computed from the DFT and AIMD simulations discussed above, both without [132] and with the effect of counter ions [133]. Their cation-free simulations [132], which sampled time scales of ~1000 s, reveal that near-neutral pH values favour linear silica oligomers, while higher pH values facilitate ring closure and faster oligomerisation. Their KMC simulations with Li^+ and NH_4^+ counter ions observe the formation of 3-rings and branched tetramers [133], with Li^+ favouring the formation of branched tetramers over 3-rings, and NH_4^+ steering more towards 3-rings. In principle, KMC allows the evolution of a complex reaction system to unfold when many competing processes make *prima facie* predictions difficult. In this case, the KMC simulations of Zhang *et al.* have predicted overall timescales and selectivities for the formation of key oligomeric species.

Simulating the formation of silica gel requires further approximations. We note that while reaction network approaches may reproduce Q_n distributions [134], these generally do not reveal atomic-level structural insights, and as such, these are not reviewed herein. Zhang *et al.* extended their KMC simulations to gel formation by making a lattice model approximation, and by assuming a simplified set of reactions and rate constants [135]. Their results predict the importance of 4-rings in both the early oligomerisation stage, and the later transition stage to gel formation. They observe 5- and 6-ring formation during the later gel-ageing stage. It is unclear whether the preference for 4-rings predicted by Zhang *et al. is* an artefact of their lattice model, which may facilitate the formation of certain structures over others depending on the lattice connectivity.

Of tangential importance to understanding how zeolites form is investigating how silica solids such as α-quartz and β-cristobalite dissolve in aqueous solution. Toward this end, Nangia and Garrison reported a series of studies applying DFT and KMC to this problem [136–138], as well as a review of the field [139]. A particular challenge in this work is characterising the surfaces of dissolving mineral species in contact with water, requiring as many as 40 possible surfaces for β-cristobalite [140]. Although the modelling work of Nangia and Garrison may shed substantial light on the physical chemistry of zeolite growth after nucleation, revealing the process of zeolite nucleation requires a study of large, amorphous silica clusters.

In 2002, Wu and Deem investigated the nucleation process of silica through an equilibrium Monte Carlo approach [141]. They calculated free energies of silica clusters of various sizes with umbrella sampling and specialised silica-grafting Monte Carlo moves. Wu and Deem predicted that in the absence of SDAs, nucleation (to some dense polymorph of SiO_2) may occur for amorphous clusters as small as 50 SiO_2 units. Their work is described in more detail in our earlier review [38]. Application of Wu and Deem's approach to include SDAs holds promise for elucidating the statistical thermodynamics of zeolite nucleation.

More recently, Deem and coworkers have reported databases of hypothetical zeolite structures as synthesis targets [44,142]. Although these databases do not speak directly to the kinetics and thermodynamics of zeolite formation, they do provide fascinating structures to compare with results of self-assembly approaches. Very recently, Deem and coworkers have reported a database of chemically synthesisable SDAs [143], switching focus from enumerating zeolite frameworks to enumerating possible SDAs. This is analogous to computational drug design, in which libraries of possible drug candidates are constructed to optimise fit in a target protein-binding pocket. Schmidt *et al.* demonstrated the power of this approach by synthesising all-silica STW zeolite using pentamethylimidazolium as the SDA [144]. Critical to this proof of principle is that pentamethylimidazolium was computationally predicted to strongly stabilise all-silica STW, while other SDAs with lower stabilisation energies did not form STW in synthesise experiments.

While this approach holds great promise for predicting SDAs for desired zeolite frameworks, the question of how zeolites nucleate and grow remains wide open.

Monson, Auerbach and coworkers have introduced several models of silica polymerisation sampled with *equilibrium* Monte Carlo simulations, neglecting the microscopic kinetics of silica condensation [128,145–148]. Our approach is inspired by the experimental Q_n distribution shown in Figure 10 (top panel). This shows that after 1 h, the Q_0 value has dropped to ~0.05 meaning that 95% of silica monomers have engaged in condensation chemistry. At this same time, $Q_3 + Q_4$ amount to ~0.1, meaning that very little three-dimensional network formation has occurred. This suggests that silica network formation may not be limited by the *microscopic* kinetics of silica condensation chemistry, but rather by collective fluctuations that produce 3D silica networks on longer length and timescales. To investigate such collective fluctuations, we have developed a series of on-lattice and off-lattice models to understand silica polymerisation and zeolite formation.

In the early 2000s, substantial experimental research pointed to the importance of silica-SDA precursor nanoparticles in zeolite formation, especially for the well-studied, clear-solution synthesis of silicalite using TPA as the SDA [95]. Although SAXS and SANS measurements showed that these nanoparticles exhibit a core–shell structure with a core rich in silica and a shell rich in TPA [92], the atomic-level structures of these particles remained poorly understood. To address these issues, Jorge *et al.* [146,149] developed a highly coarse-grained simple cubic lattice model of silica condensation and silica-TPA association. This work was described in some detail in our earlier review [38]; here, we touch on its major findings. Using united-atom descriptions of neutral and anionic silica monomers and of TPA, this lattice model successfully and simply described the self-assembly via Ostwald ripening of silica-TPA nanoparticles with the same core–shell structure found in experiments. These nanoparticles were found in our simulations to be metastable, in excellent agreement with experiments of Davis *et al.* [37].

This model was extended in 2010 by Jin *et al.* [150] with the same level of coarse graining to the body-centred cubic (bcc) lattice, which contains two interpenetrating tetrahedral lattices, and as such fits well with the tetrahedral nature of bonding in $Si(OH)_4$. Using the bcc lattice allows silica monomers to fluctuate on one tetrahedral sublattice, and TPA species to fluctuate on the other, producing the concept of pore spaces. Jin *et al.* found that the TPA loading of these core–shell nanoparticles was quite comparable to the amount of TPA in as-synthesised silicalite, a remarkable success for this simple model. However, the amount of TPA penetration into the silica core, a necessary step for zeolite formation, was found to be negligible [150]. These results remind us that simple models can be quite effective at addressing complex systems, but that successively more sophisticated models are required to predict important structural details.

In 2011, Jin *et al.* reported a new lattice model of silica polymerisation with *atomic-level detail*, based on $Si(OH)_4$ tetrahedra fluctuating on a bcc lattice (see Figure 11) [128]. This new silica model represents a breakthrough in our ability to sample silica networks, allowing its wide application in other contexts [151,152]. The essence of the model involves the following: (i) atomic resolution of silica monomers allowing various Si–O–Si angles (in contrast to our previous work with higher levels of coarse graining [146,150]); (ii) fluctuations restricted to translations and/or rotations of intact $Si(OH)_4$ tetrahedra; (iii) ‘Glauber’ dynamics meaning that translations to any lattice vacancy are allowed in one step; and (iv) condensation chemistry represented by allowing double occupancy of OH groups from adjacent tetrahedra, producing a stabilisation energy associated with the exothermicity of silica condensation, and a lattice vacancy representing the resulting water molecule.

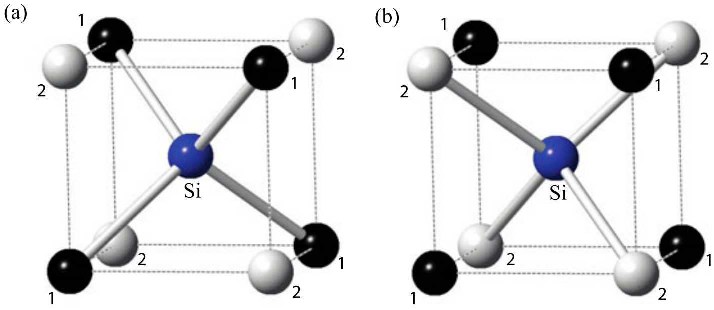

Figure 11. (Colour online) $Si(OH)_4$ monomers in various configurations on a body-centred cubic (bcc) lattice model (Reprinted with permission from Jin *et al.* [128] Copyright (2011) AIP Publishing LLC).

This remarkably simple model sampled with canonical Monte Carlo yields the simulated Q_n distribution shown in Figure 10 (bottom), in nearly complete agreement with the experimental NMR results (top). As a technical point, we note that because equilibrium Monte Carlo lacks a proper measure of physical time, we have aligned the two graphs in Figure 10 using the crossing points in the Q_0 and Q_1 traces. What is remarkable in Figure 10 is that after this crossing point (at a physical time of about 0.1 h), experiment and Monte Carlo remain in very good agreement, suggesting that each Monte Carlo step corresponds to a constant amount of physical time, in this case about 4 min. The ability of our model to faithfully reproduce the Q_n distribution, while wholly ignoring the microscopic details of silica condensation kinetics and monomer mass transport, suggests that network formation in silica gel is ultimately controlled by collective fluctuations at longer length scales, and that our model samples these fluctuations with reasonable fidelity.

The success of this atomic lattice model of silica polymerisation has opened the door to studying self-assembly of more complex and interesting systems, as discussed below. However, one thing this lattice model cannot accomplish is modelling zeolite formation, because no known zeolite framework fits onto the bcc lattice. (As an aside, we note that the idealised β-cristobalite structure and several chalcogenides do fit onto the bcc lattice, as exploited by Jin *et al.* [151]). As such, we seek an off-lattice model of silica that can reproduce the evolution of the Q_n distribution, and eventually, can capture the stages of zeolite nucleation. We accomplished the former as reported in Malani *et al.* [147,148] involving the assembly of flexible $Si(OH)_4$ tetrahedra with reactive ensemble Monte Carlo simulations, which obviates the need to specify a reactive forcefield. These simulations are distinguished by the following collection of Monte Carlo moves: translation and rotation of tetrahedra, intramolecular distortion of tetrahedra, cluster moves with probabilities following Stokes-Einstein diffusivities, and intracluster condensations (producing rings) facilitated by force-bias relaxation of target structures. The resulting Q_n distribution shows excellent agreement with NMR data, and analyses of cluster-size and ring-size distributions reveal that polymerisation proceeds in the following main stages: oligomerisation forming small units (0–1 h), ring formation (1–2.6 h), cluster aggregation (2.6–5.6 h) and finally, cross-linking of the ageing gel at later times. The simulations further indicate a predominance of 4-, 5- and 6-rings, and a fractal dimension of the silica gel of 2.0. This off-lattice

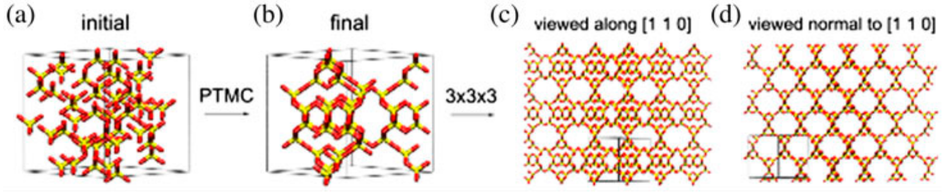

Figure 12. (Colour online) Results of parallel tempering Monte Carlo (PTMC) simulations showing self-assembly of a crystalline nanoporous zeolite analogue with two interpenetrating 12-ring channels in an 8 × 8 × 8 unit bcc lattice. (a,b) Initial (random) and final configurations from PTMC. (c,d) 3 × 3 × 3 periodic extensions of that in b), viewed along and normal-to the [110] direction, respectively. The black lines indicate simulation cell boundaries; (Reprinted with permission from Jin *et al.* [151]. Copyright (2012) American Chemical Society).

model is similar in spirit to that of Wu and Deem [141] extending both models to include SDAs represents a fruitful avenue for future research.

Despite the *substantial* amount of molecular modelling research on the formation of ordered nanoporous silica materials, no statistical mechanics-based simulation had produced the self-assembly of nanoporous crystals until the work of Jin *et al.* in 2012 [151]. In this work, we simulated the atomic lattice model of silica discussed above [128] using parallel tempering Monte Carlo (PTMC), which involves running Monte Carlo simulations on several system replicas at various temperatures and attempting swaps between replicas with an acceptance probability that maintains the overall detailed balance. Swapping systems between different temperatures is reminiscent of annealing, and hence allows systems to overcome free energy barriers precluding proper equilibration. When running canonical Monte Carlo with this lattice model initialised randomly with a lattice coverage of $x_\beta = 0.0625$, corresponding to that of the idealised β-cristobalite structure, we found the formation of silica gel with one large, amorphous pore. However, when running with PTMC, we found the formation of crystalline β-cristobalite. When running PTMC at lower lattice coverages (e.g. see Figure 12 with $x = 0.04688 = 0.75x_\beta$), we found the emergence of several crystalline zeolite analogues. In addition, this remarkably simple model also produces a rich array of layered materials as well as known nanoporous chalcogenides. It remains to be seen how including SDAs in these PTMC simulations may influence the evolution of structure from random initial conditions to the vast array of available zeolite analogues. It is also interesting to investigate the connectivities of these zeolite analogues, and how 'close' they are to hypothetical zeolites in online databases [44,153].

6. Modelling ordered mesoporous silica synthesis

Modelling ordered mesoporous silica materials synthesis poses several challenges. In particular. it involves multiple length scales. The mesophase ordering is on the length scale of a few nm to tens of nm, while the detailed structure of the interfaces in the systems and the atomic structure of the assembled silica involve sub-nanometer scale. Key questions are the nature of the mesophase assembly:

- How do the silica and surfactant interact to produce the mesophase assembly?
- What is the extent of polymerisation in the silica during the mesophase assembly?

There have been several very interesting modelling studies of self-assembly of ordered mesoporous silica materials using molecular simulation techniques. Three major lines of attack can be seen in this work. Siperstein and Gubbins [154] built a lattice model of the system that made use of the Larsen lattice model of surfactants [155]. They were able to observe self-assembly of the silica particles into cylinders generating a structure similar to that of MCM-41. The focus here is on the overall structure of the mesophases formed, which can be addressed in a coarse-grained model like this one. The model of silica used does not include the low coordination interactions necessary to generate a realistic model of either amorphous or crystalline silica. Additional studies of this approach have been reported by Siperstein and her coworkers [156–160].

Off-lattice models lead to a more realistic picture of structure than lattice models at the cost of additional expense. In one approach to this, a model of silica polymerisation in the context of constraints created by an assumed pore structure. This is exemplified by the work of Schumacher *et al.* [161] and leads to a good model of density in the core of the solid phase in the porous material. However, the enforcement of rigid boundaries eliminates the possibility of accounting for variations in the pore size and shape that will be created by interfacial fluctuations during the self-assembly process. Gubbins and coworkers [162,163] have used the lattice model of self-assembly to generate off-lattice models by taking a model of cristobalite and carving out pores with the geometry of those determined from the lattice model. In their most recent work, they have studied SBA-15 and introduced a method to carve out micropores as well as mesopores [162]. This allows for inclusion of interfacial fluctuations into the pore wall structure but the silica polymerisation is still assumed to be decoupled from the mesophase formation.

An alternative to the above models are fully atomistic models of the silica-surfactant self-assembly system. Seaton and Jorge [164,165] have used all-atom models of the water-surfactant–silica system to study the early stages of the process of templated self-assembly. Models like this can provide significant level of detail about the effects of specific interactions in the system, for example, the tendency of the silica to adsorb in the exterior surface of the surfactant micelles. On the other hand, such models are limited both by the size of the system that can be used and the timescale over which the phenomena can be studied.

Recently, Perez-Sanchez *et al.* [166] have introduced a coarse-grained off-lattice model of surfactant–water–silica self-assembly and were able to show how addition of silica to a water surfactant system with spherical micelles led to the formation of rod-like micelles in the system. This approach will be promising if it can be combined with a suitable model of silica polymerisation to give realistic models of OMS pore structure.

Until recently for modelling ordered mesoporous silica formation at suitably large length scales, the state-of-the-art methods focused either on the silica polymerisation [161] or the mesophase self-assembly [154]. We will now discuss the work of Jin *et al.* [152] where both these aspects are addressed in combination. Jin *et al.* [152] combined the surfactant lattice model of Larson [167], together with a tetrahedral lattice model of silica [128] to make a model of the surfactant templating of OMS's. Surfactant molecules were represented as H_iT_j, with i hydrophilic head groups (H) and j hydrophobic tail groups [167] (T) occupying chains of connected simple cubic lattice sites, as shown in Figure 13. The Monte Carlo moves of surfactant molecules include chain reptation, cluster move, partial and complete chain regrowth using configurational-bias Monte Carlo [168]. They first simulated the H_4T_4-solvent binary system over a range of H_4T_4

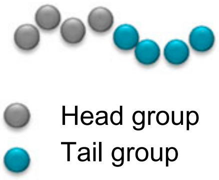

Figure 13. (Colour online) Representation of a H_4T_4 model surfactant in Larson's model [167].

volume fractions. At certain volume fractions, they carried out canonical ensemble simulations at various temperatures and recorded the highest temperature at which ordered phases formed. The H_4T_4-solvent phase diagram is plotted in Figure 14(a),

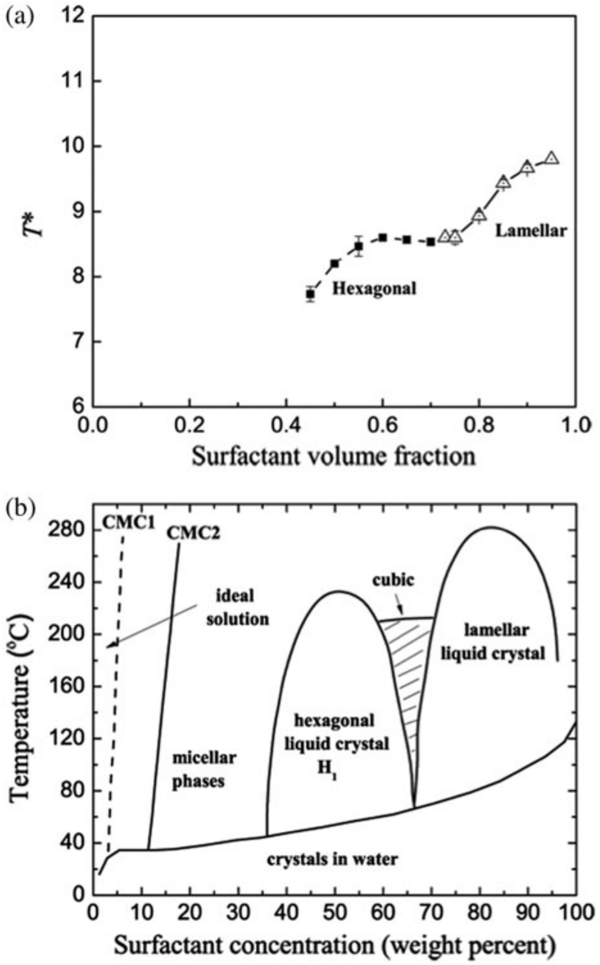

Figure 14. Phase diagram for surfactant–solvent system. (a) Phase diagram for H_4T_4-solvent system. Symbols are results from Canonical Ensemble Monte Carlo simulations. ■ Hexagonal phases; △ Lamellar phases. Lines are plotted to guide the eye. (b) Schematic phase diagram for C_{16}TMABr in water, data points were taken from Brinker *et al.* (Adapted with permission from Jin *et al.* [152]. Copyright (2013) American Chemical Society).

while Figure 14(b) shows the schematic phase diagram of C_{16}TMABr in water from experiments, and data points were taken from Brinker *et al.* [169] The interchange energy ε_{HT} was calibrated by comparing the highest temperatures to form the hexagonal phases from simulations and experiments. Since, the overall behaviour of silica solutions are greatly affected by the solution pH [134] and the influence of pH was taken into account using reaction ensemble Monte Carlo simulations [170].

The liquid crystalline phases can be formed under conditions where silicates alone do not condense (solution pH of 12–14 and concentration of the surfactant is within 0.5–5%, below the concentration at which forms the liquid crystalline phases [24]). Electron paramagnetic resonance spectroscopy measurements suggested that the hexagonal long-range ordering formed at least 10 times faster than condensation of silicates that compose the inorganic phases [171]. Therefore, a ‘two-step synthesis’ methodology was adopted for simulating the formation of mesoporous silica materials. During first step, no silica condensation reaction was considered and this simulation stage corresponds to the experimental conditions of high solution pH and low temperature.

After the mesostructures are formed with long-range ordering, the second step with explicit representation of inorganic species condensation and silicate deprotonation reaction takes place. This step resembles the neutralisation step during experimental synthesis: the silicic condensation kinetics were greatly accelerated at lower pH and higher temperature.

Jin *et al.* [152] first investigated the role of silicate by gradually increasing the concentration of silica, while keeping the fraction of H_4T_4 constant. All simulations were carried out under conditions where inorganic species condensation is negligible. As the concentration of H_4T_4 (volume fraction of 7.5%) exceeded the critical micelle concentration, spherical micelles were formed in binary H_4T_4-solvent system. The concentration of surfactants falls into the micelle formation region, consistent with the experimental phase diagram of C_{16}TMABr aqueous solution (Figure 14).

When a small amount of silicate species was added into the system, silica molecules were attracted to the surface of surfactant micelles due to the strong affinity between ionic silica and head groups of surfactant, as shown in Figure 15(b). When enough inorganic species were added to the system, the system phase separated into a surfactant-inorganic concentrated phase in equilibrium with solvent-rich phase. Figure 15(c) depicts the snapshot of the system and mesostructures composed of hexagonal array of cylinders are seen. These simulations support the cooperative templating mechanism indicating that silica tetrahedra play an important role in the mesophase assembly during the formation of mesoporous materials. They were also able to observe a reversible hexagonal to lamellar morphology by changing the temperature. This had been observed experimentally by Firouzi *et al.* [26].

Zana and coworkers [172] have reported fluorescence data that they interpret as showing halide counterions outcompete silicate anions for interactions with surfactant head groups, calling into question our assumption that adding silica to the surfactant system at high pH will necessary produce silica-surfactant complexes. We ignore such halide counter ions in our simulations, based on the assumption that halides are more soluble in water than are silicates. More experimental and modelling work is needed to address this important step in silica-surfactant assembly.

Turning now to the two-step synthesis process, Figure 16(a) depicts the initial configuration with surfactant (H_4T_4) and silicate molecules randomly distributed in a 30 × 30 × 240 box. When the canonical ensemble simulations were carried out, surfactant molecules tend to form micelles with hydrophobic tail groups gathering inside and

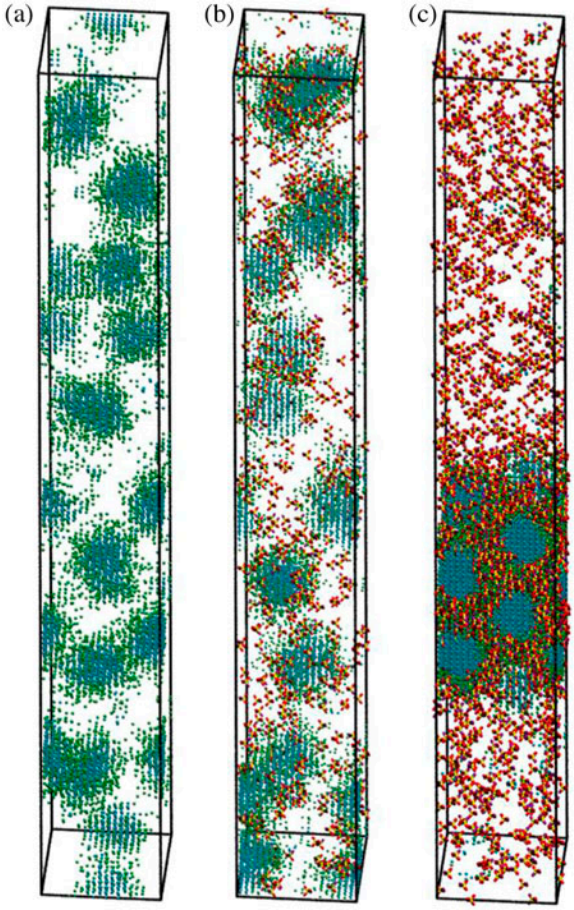

Figure 15. (Colour online) Phase separation when silica is added into the H_4T_4-solvent system, $T^* = 6.5$, system size 20 × 20 × 160. (a) Spherical micelles formed in binary surfactant–solvent system, at $c_{H4T4} = 0.009375$. (b) and (c) Ternary surfactant–silica–solvent system with the same volume fraction of H_4T_4 as (a), but increased concentration of silica. (b) $c_{SI} = 0.005$ (c) $c_{SI} = 0.015$. Blue and green spheres represent tail and head groups of surfactant molecules; red and purple spheres illustrate neutral and negatively charged oxygens, and yellow spheres at the centre of silica tetrahedra show silicon atoms (Adapted with permission from Jin *et al.* [152]. Copyright (2013) American Chemical Society).

hydrophilic head groups facing outside, and silicate species were strongly attracted to the head segments. Due to the assumed strong interaction between silica and the surfactant head group, the system phase separated into a surfactant–silicate-rich phase in equilibrium with a solvent phase. The dense phase was found with mesoscale ordering possessing a hexagonal array of pores occupied by tails segments, as shown in Figure 16(b). The above observation is consistent with previous lattice model MC studies [173] and experimental observations.[26] The final configuration in Figure 16(b) was the starting point of step two, where silica polymerisation and silica deprotonation reactions were considered when decrease solution pH and/or increase system temperature in real synthesis. During this approach, silicate species continue to polymerise and condense. Snapshots taken before and after the condensation step are seen in

Figure 16(b) and c, respectively, for comparison. Figure 16(d) shows only the silicate species after removal of the surfactant, mimicking the calcination procedure that removes the template molecules and makes the pore space available.

In reality, under modest solution pH and elevated temperatures where the kinetics of surfactant assembly and silica condensation are comparable, the two step assumption is invalid. More efforts need to be paid to rationalise the relative timescales for these chemical reactions and self-assembly processes. One extreme case involves the experiments carried out by Beck *et al.* [15] in which high temperatures were chosen such that the silicate condensation reaction is much faster. We simulated this process with MC moves including simultaneously surfactant assembly, silicate molecule transportation and rotation, and silicate condensation and deprotonation reactions. Because of the rapid polymerisation of inorganic species, the final product lacks long-range ordering and only amorphous silica is formed (Figure 16(e)), in agreement with experimental phenomena observed by Beck *et al.* [15] They showed that at 200 °C, only zeolitic and dense phase products can be obtained probably due to the fast polymerisation of silicate species which formed the scaffolds and hindered the longer range ordering.

The work of Jin *et al.* shows that we are now in a position to model both the mesophase self-assembly and silica polymerisation in these systems using a lattice based approach. Nevertheless, a great deal of work remains to be done. In the context of the Jin approach, more extensive calculations with longer tail groups would be useful. This would permit the model synthesis of systems with wider pores and investigation of the pore wall structure. Issues such as the microporosity in the pore walls (e.g. in SBA-15) could then be investigated. Another question concerns the degree of polymerisation of the silica during the mesoscale self-assembly of the surfactant–water–silica system. The Jin model assumes only the presence of silica monomers. As a practical matter, this situation cannot be realised experimentally and it is important to investigate the effect of the presence of silica oligomers upon the process.

7. Summary and outlook

In this review, we have described recent progress in the modelling of the formation of nanoporous silica materials with an emphasis on zeolite framework materials and ordered silica mesoporous materials. We have reviewed several modelling approaches that have contributed to an improvement of our understanding of these processes. An essential component of how to model these systems is an understanding of silica polymerisation in the presence of structure directing agents. We have seen how significant progress can be made by considering models of this polymerisation based on the assembly of corner-sharing tetrahedra. We conclude our review by addressing some of the remaining challenges for modelling work in this area and to experimentation, and suggesting some areas where we can expect progress in modelling and applications to still wider ranges of porous materials.

Many of the remaining challenges in this area are in a sense common to both modelling and experiment. Key to understanding both micropore and mesopore formation is identifying key intermediate silica-SDA structures that lead to nanopore formation. In the case of zeolite formation, developing new modelling methods and experimental *in situ* characterisation techniques are crucial for peering into the nanoscale blindspot of zeolite nucleation. On the experimental side, recent studies have succeeded in bracketing length scales of zeolite nucleation into the range 5–10 nm, although determining precise structures for zeolite nuclei remains an outstanding challenge. On the modelling

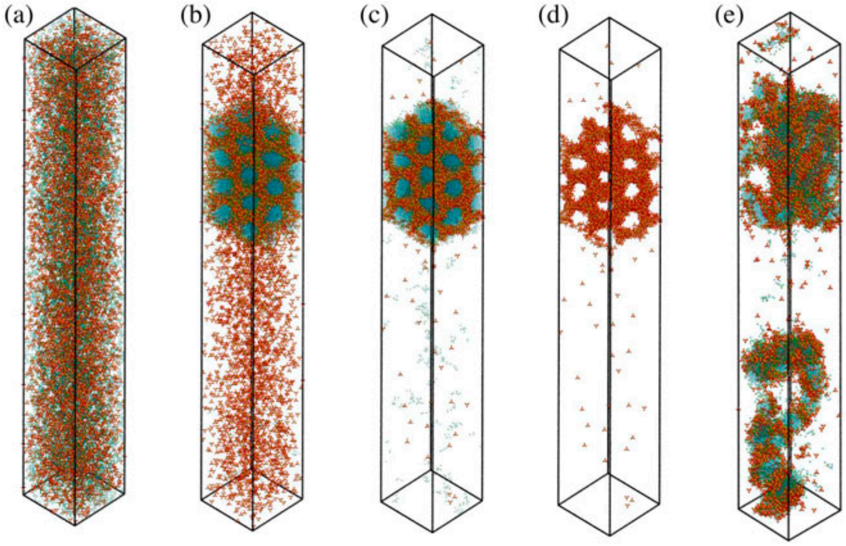

Figure 16. (Colour online) Simulating the two-step formation of ordered mesoporous silica materials, at $T^* = 6.5$, box size of 30 × 30 × 240. $c_{\mathrm{H4T4}=}0.009375$ and $c_{\mathrm{Silica}} = 0.015$ (a) Initial configuration with 4050 H_4T_4 and 6480 ionic silica S_I randomly distributed in the simulation box. (b) Final configuration of step one. Snapshot taken in direction where hexagonal array of cylindrical pores are shown. Monte Carlo simulations were carried out under conditions that silicate polymerisation is negligible. (b) is also the starting configuration of step two. (c) Snapshot of final configuration of step two. (d) Only silicate species were shown from snapshot (c). (e) Instead of using the two-step synthesis method, a one-step synthesis scheme that allows simultaneous silicate polymerisation, silica deprotonation and surfactant assembly was utilised with a random initial configuration. A much more disordered structure is obtained. (Adapted with permission from Jin *et al.* [152]. Copyright (2013) American Chemical Society).

side, it remains unclear whether kinetic models, thermodynamic models, or hybrid models may elucidate nucleation. While the quantum chemistry modelling of Van Santen and coworkers suggests that kinetics are crucial for understanding the microscopic processes of silica condensation, the Monte Carlo simulations of Auerbach, Monson, and coworkers indicate that the formation of 3D silica networks may *not* be controlled by microscopic kinetics, but rather by network fluctuations on longer length scales successfully treated by coarse-grained models. We believe that the future of this field lies in identifying the *minimum* amount of atomic level and kinetic detail necessary to capture the physics of zeolite nucleation.

In the case of mesopore formation, as we have noted in the previous section, it is important to understand the relative rates of mesophase formation and silica polymerisation at different types of conditions, where porous materials synthesis is carried out. This is a challenge for experiment, especially in the context of tracking polymerisation kinetics within silica clusters. At the same time, the models that we have described for the formation of nanoporous silica materials are based on cluster formation or mesophase self-assembly in the absence of silica polymerisation, followed by silica polymerisation once the mesophase structure is in place. It seems likely that there is at least some degree of oligomerisation taking place, while cluster formation or mesophase self-assembly are occurring. Gaining a deeper understanding of the relative kinetics of mesoscale formation and silica condensation – from both experiments and molecular modelling – will be crucial quantitative control of this mesoscale assembly process.

As reviewed above, significant progress has been made over the past decade in unifying the kinds of models used to understand micropore and mesopore formation. Energy minimisations of putative SDAs in known zeolite pores have typically been used to 'understand' zeolite formation, while more coarse-grained models of self-assembly have been used productively to shed light on mesopore formation. In contrast to this previous state of affairs, we have described above a new paradigm involving a single, common modelling framework for understanding both zeolite and silica mesopore formation. We believe this represents a substantial step forward, opening the door to a much fuller understanding of how these materials form, and what new, tailor-made materials may lie ahead.

The present article has focused on silica polymerisation, zeolite formation and ordered mesoporous materials formation. We believe that the lessons obtained from the work described, here, may find application in areas outside of those discussed here. Hierarchical materials, such as the recently synthesised mesoporous-microporous zeolite systems, represent a nexus of microporous crystalline materials and ordered mesoporous materials. The concept of assembly through low coordination number-bonding units (corner-sharing tetrahedra) that we have seen for silica materials are likely also applicable to other systems. In particular, we anticipate future applications to carbon materials and to metal-organic framework materials. We look forward to the many developments in this field that are likely in the years ahead.

Acknowledgements

Research by PAM and SMA has been supported by the Department of Energy (Contract No. DEFG02-07ER46466). Research by WF is partially supported by the Catalysis Center for Energy Innovation, an Energy Frontier Research Center funded by the U.S. Department of Energy, Office of Science and Office of Basic Energy Sciences under Award No. DE-SC0001004. PAM and SMA are grateful for contributions to this research by several coworkers: Roope Astale, Matt Ford, Miguel Jorge, Lin Jin, Atteeque Malani, Szu-Chia Chien, Navaid Khan and German Perez-Sanchez.

References

[1] M.E. Davis, Nature **417**, 813 (2002).
[2] A. Corma, Chem. Rev. **97**, 2373 (1997).
[3] M.A. Snyder and M. Tsapatsis, Angew. Chem. Int. Ed. **46**, 7560 (2007).
[4] M. Vallet-Regí, F. Balas and D. Arcos, Angew. Chem. Int. Ed. **46**, 7548 (2007).
[5] M. Hartmann, Chem. Mater. **17**, 4577 (2005).
[6] K. Nakanishi and N. Tanaka, Acc. Chem. Res. **40**, 863 (2007).
[7] J.W. Zhao, F. Gao, Y.L. Fu, W. Jin, P.Y. Yang and D.Y. Zhao, Chem. Commun. 752, (2002).
[8] Z.B. Wang, H.T. Wang, A. Mitra, L.M. Huang and Y.S. Yan, Adv. Mater. **13**, 746 (2001).
[9] S.M. Auerbach, K.A. Karrado and P.K. Dutta, editors, *Handbook of Zeolite Science and Technology* (Marcel Dekker, New York, 2003), p. 1184.
[10] C. Baerlocher, L.B. McCusker and D.H. Olson, *Atlas of Zeolite Framework Types*, 6th ed. (Elsevier, Amsterdam, 2007).
[11] R. Brent, P. Cubillas, S.M. Stevens, K.E. Jelfs, A. Umemura, J.T. Gebbie, B. Slater, O. Terasaki, M.A. Holden and M.W. Anderson, J. Am. Chem. Soc. **132**, 13858 (2010).

[12] V. Alfredsson, T. Ohsuna, O. Terasaki and J.O. Bovin, Angew. Chem. Int. Ed. **32**, 1210 (1993).

[13] C.S. Yang, J.M. Mora-Fonz and C.R.A. Catlow, J. Phys. Chem. C. **117**, 24796 (2013).

[14] T. Yanagisawa, T. Shimizu, K. Kuroda and C. Kato, Bull. Chem. Soc. Jpn. **63**, 988 (1990).

[15] J.S. Beck, J.C. Vartuli, W.J. Roth, M.E. Leonowicz, C.T. Kresge, K.D. Schmitt, C.T.W. Chu, D.H. Olson, E.W. Sheppard, S.B. McCullen, J.B. Higgins and J.L. Schlenker, J. Am. Chem. Soc. **114**, 10834 (1992).

[16] M. Manzano and M. Vallet-Regí, J. Mater. Chem. **20**, 5593 (2010).

[17] S. Wang, Microporous Mesoporous Mater. **117**, 1 (2009).

[18] C.T. Kresge, M.E. Leonowicz, W.J. Roth, J.C. Vartuli and J.S. Beck, Nature **359**, 710 (1992).

[19] G.S. Attard, J.C. Glyde and C.G. Göltner, Nature **378**, 366 (1995).

[20] J.S. Beck, J.C. Vartuli, G.J. Kennedy, C.T. Kresge, W.J. Roth and S.E. Schramm, Chem. Mater. **6**, 1816 (1994).

[21] C.-Y. Chen, S.L. Burkett, H.-X. Li and M.E. Davis, Microporous Mater. **2**, 27 (1993).

[22] C.Y. Chen, H.X. Li and M.E. Davis, Microporous Mater. **2**, 17 (1993).

[23] A. Firouzi, D. Kumar, L.M. Bull, T. Besier, P. Sieger, Q. Huo, S.A. Walker, J.A. Zasadzinski, C. Glinka, J. Nicol, D. Margolese, G.D. Stucky and B.F. Chmelka, Science **267**, 1138 (1995).

[24] A. Monnier, F. Schuth, Q. Huo, D. Kumar, D. Margolese, R.S. Maxwell, G.D. Stucky, M. Krishnamurty, P. Petroff, A. Firouzi, M. Janicke and B.F. Chmelka, Science **261**, 1299 (1993).

[25] I. Beurroies, P. Ågren, G. Büchel, J.B. Rosenholm, H. Amenitsch, R. Denoyel and M. Linden, J. Phys. Chem. B. **110**, 16254 (2006).

[26] A. Firouzi, F. Atef, A.G. Oertli, G.D. Stucky and B.F. Chmelka, J. Am. Chem. Soc. **119**, 3596 (1997).

[27] R.F. Lobo, in *Handbook of Zeolite Science and Technology*, edited by Scott Auerbach, Kathleen Carrado and Prabir Dutta (Marcel-Dekker, New York, 2003), pp. 65–65.

[28] P.D. Yang, D.Y. Zhao, D.I. Margolese, B.F. Chmelka and G.D. Stucky, Nature **396**, 152 (1998).

[29] D. Zhao, J. Feng, Q. Huo, N. Melosh, G. Fredrickson, B. Chmelka and G. Stucky, Science **279**, 548 (1998).

[30] M.E. Davis and R.F. Lobo, Chem. Mater. **4**, 756 (1992).

[31] S. Kumar, Z.P. Wang, R.L. Penn and M. Tsapatsis, J. Am. Chem. Soc. **130**, 17284 (2008).

[32] S. Kumar, T.M. Davis, H. Ramanan, R.L. Penn and M. Tsapatsis, J. Phys. Chem. B. **111**, 3398 (2007).

[33] P. de Moor, T.P.M. Beelen and R.A. van Santen, J. Phys. Chem. B. **103**, 1639 (1999).

[34] W. Fan, M. Ogura, G. Sankar and T. Okubo, Chem. Mater. **19**, 1906 (2007).

[35] W. Fan, M. O'Brien, M. Ogura, M. Sanchez-Sanchez, C. Martin, F. Meneau, K. Kurumada, G. Sankar and T. Okubo, Phys. Chem. Chem. Phys. **8**, 1335 (2006).

[36] W. Fan, F. Meneau, W. Bras, M. Ogura, G. Sankar and T. Okubo, Microporous Mesoporous Mater. **101**, 134 (2007).

[37] T.M. Davis, T.O. Drews, H. Ramanan, C. He, J.S. Dong, H. Schnablegger, M.A. Katsoulakis, E. Kokkoli, A.V. McCormick, R.L. Penn and M. Tsapatsis, Nat. Mater. **5**, 400 (2006).

[38] S.M. Auerbach, M.H. Ford and P.A. Monson, Curr. Opin. Colloid Interface Sci. **10**, 220 (2005).

[39] R. Astala, S.M. Auerbach and P.A. Monson, J. Phys. Chem. B. **108**, 9208 (2004).

[40] G.K. Johnson, I.R. Tasker, D.A. Howell and J.V. Smith, J. Chem. Thermodyn. **19**, 617 (1987).

[41] P.M. Piccione, C. Laberty, S.Y. Yang, M.A. Camblor, A. Navrotsky and M.E. Davis, J. Phys. Chem. B. **104**, 10001 (2000).

[42] M.D. Foster and M.M.J. Treacy, *A Database of Hypothetical Zeolite Structures*. <http://www.hypotheticalzeolites.net>.

[43] M.W. Deem, *Database of Hypothetical Zeolite Structures*. <http://www.hypotheticalzeolites.net/DATABASE/DEEM/index.php>.

[44] D.J. Earl and M.W. Deem, Ind. Eng. Chem. Res. **45**, 5449 (2006).

[45] D. Kuang, T. Brezesinski and B. Smarsly, J. Am. Chem. Soc. **126**, 10534 (2004).

[46] O. Sel, D. Kuang, M. Thommes and B. Smarsly, Langmuir **22**, 2311 (2006).

[47] M. Thommes, B. Smarsly, M. Groenewolt, P. Ravikovitch and A. Neimark, Langmuir **22**, 756 (2006).

[48] K. Na, C. Jo, J. Kim, K. Cho, J. Jung, Y. Seo, R.J. Messinger, B.F. Chmelka and R. Ryoo, Science **333**, 328 (2011).

[49] W. Fan, M.A. Snyder, S. Kumar, P.-S. Lee, W.C. Yoo, A.V. McCormick, R.L. Penn, A. Stein and M. Tsapatsis, Nat. Mater. **7**, 984 (2008).

[50] M.T. Dove, V. Heine and K.D. Hammonds, Mineral. Mag. **59**, 629 (1995).

[51] K.D. Hammonds, V. Heine and M.T. Dove, J. Phys. Chem. B. **102**, 1759 (1998).

[52] R.M. Barrer, *Hydrothermal Chemistry of Zeolites* (Academic Press, London, 1982).

[53] R.K. Iler, *The Chemistry of Silica: Solubility, Polymerization, Colloid and Surface Properties, and Biochemistry* (Wiley, New York, 1979). p. xxiv.

[54] C.J. Brinker and G.W. Scherer, *Sol–Gel Science: The Physics and Chemistry of Sol–Gel Processing* (Academic Press, Boston, MA, 1990). p. xiv.

[55] R.J.P. Corriu and D. Leclercq, Angew. Chem. Int. Ed. **35**, 1420 (1996).

[56] A.M. Buckley and M. Greenblatt, J. Chem. Educ. **71**, 599 (1994).

[57] C.T.G. Knight, R.J. Kirkpatrick, and E. Oldfield, J. Magn. Reson. **78**, 31 (1988).

[58] C.J. Brinker, D.E. Clark and D.R. Ulrich, *Better Ceramics Through Chemistry II Symposium*, April 15-19, 1986, Palo Alto, CA, USA, in Materials Research Society Symposia Proceedings (Materials Research Society, Pittsburgh, PA, 1988). p. 1 online resource (xvii).

[59] G. Engelhardt, W. Altenburg, D. Hoebbel and W. Wieker, Z. Anorg. Allg. Chem. **437**, 249 (1977).

[60] C.J. Brinker, K.D. Keefer, D.W. Schaefer, R.A. Assink, B.D. Kay and C.S. Ashley, J. Non-Cryst. Solids **63**, 45 (1984).

[61] C.J. Brinker, K.D. Keefer, D.W. Schaefer and C.S. Ashley, J. Non-Cryst. Solids **48**, 47 (1982).

[62] T. Matsoukas and E. Gulari, J. Colloid Interface Sci. **145**, 557 (1991).

[63] T. Matsoukas and E. Gulari, J. Colloid Interface Sci. **132**, 13 (1989).

[64] T. Matsoukas and E. Gulari, J. Colloid Interface Sci. **124**, 252 (1988).

[65] S. Kim and C.F. Zukoski, J. Colloid Interface Sci. **139**, 198 (1990).

[66] G.H. Bogush and C.F. Zukoski, J. Colloid Interface Sci. **142**, 19 (1991).

[67] G.H. Bogush and C.F. Zukoski, J. Colloid Interface Sci. **142**, 1 (1991).

[68] A. Vanblaaderen, J. Vangeest and A. Vrij, J. Colloid Interface Sci. **154**, 481 (1992).

[69] F. Hoffmann, M. Cornelius, J. Morell and M. Fröba, Angew. Chem. Int. Ed. **45**, 3216 (2006).

[70] Y. Wan and D.Y. Zhao, Chem. Rev. **107**, 2821 (2007).

[71] J.L. Blin and M. Impéror-Clerc, Chem. Soc. Rev. **42**, 4071 (2013).

[72] G.S. Attard, J.C. Glyde and C.G. Göltner, Nature **378**, 366 (1995).

[73] Q. Huo, D.I. Margolese, U. Ciesla, P. Feng, T.E. Gier, P. Sieger, R. Leon, P.M. Petroff, F. Schüth and G.D. Stucky, Nature **368**, 317 (1994).

[74] D. Zhao, J. Feng, Q. Huo, N. Melosh, G.H. Fredrickson, B.F. Chmelka and G.D. Stucky, Science **279**, 548 (1998).

[75] S.A. Bagshaw, E. Prouzet and T.J. Pinnavaia, Science **269**, 1242 (1995).

[76] P.T. Tanev and T.J. Pinnavaia, Science **267**, 865 (1995).

[77] R.M. Barrer, J.W. Baynham, F.W. Bultitude and W.M. Meier, J. Chem. Soc. 195, (1959).

[78] D.W. Breck, *Zeolite Molecular Sieves* (John Wiley and Sons, New York, 1974).

[79] G.T. Kerr, J. Phys. Chem. **70**, 1047 (1966).

[80] G.T. Kerr, Inorg. Chem. **5**, 1537 (1966).

[81] G.T. Kerr, Inorg. Chem. **5**, 1539 (1966).

[82] R.M. Barrer and P.J. Denny, J. Chem. Soc. 971, (1961).

[83] G.T. Kerr and Gt. Kokotailo, J. Am. Chem. Soc., **83**, 4675 (1961)

[84] R.L. Wadlinger, G.T. Kerr and E.J. Rosinski, Google Patents (1967).

[85] R.L. Argauer and G.R. Landolt, Google Patents (1972).

[86] A. Corma, M.J. Díaz-Cabañas, J.L. Jordá, C. Martínez and M. Moliner, Nature **443**, 842 (2006).

[87] S.I. Zones, A.W. Burton, G.S. Lee and M.M. Olmstead, J. Am. Chem. Soc. **129**, 9066 (2007).

[88] M.E. Davis, Chem. Mater. **26**, 239 (2013).

[89] C.D. Chang and A.T. Bell, Catal. Lett. **8**, 305 (1991).

[90] S.L. Burkett and M.E. Davis, J. Phys. Chem. **98**, 4647 (1994).

[91] P. de Moor, T.P.M. Beelen, B.U. Komanschek, L.W. Beck, P. Wagner, M.E. Davis and R.A. van Santen, Chem. Eur. J. **5**, 2083 (1999).

[92] J.M. Fedeyko, J.D. Rimer, R.F. Lobo and D.G. Vlachos, J. Phys. Chem. B. **108**, 12271 (2004).

[93] M.A. Snyder, J.A. Lee, T.M. Davis, L.E. Scriven and M. Tsapatsis, Langmuir **23**, 9924 (2007).

[94] S. Kumar, R.L. Penn and M. Tsapatsis, Microporous Mesoporous Mater. **144**, 74 (2011).

[95] V. Nikolakis, E. Kokkoli, M. Tirrell, M. Tsapatsis and D.G. Vlachos, Chem. Mater. **12**, 845 (2000).

[96] N.D. Hould and R.F. Lobo, Chem. Mater. **20**, 5807 (2008).

[97] V.P. Valtchev and K.N. Bozhilov, J. Phys. Chem. B. **108**, 15587 (2004).

[98] N.D. Hould, S. Kumar, M. Tsapatsis, V. Nikolakis and R.F. Lobo, Langmuir **26**, 1260 (2010).

[99] I. Petrovic, A. Navrotsky, M.E. Davis and S.I. Zones, Chem. Mater. **5**, 1805 (1993).

[100] P.M. Piccione, C. Laberty, S. Yang, M.A. Camblor, A. Navrotsky and M.E. Davis, J. Phys. Chem. B. **104**, 10001 (2000).

[101] A. Navrotsky, O. Trofymluk and A.A. Levchenko, Chem. Rev. **109**, 3885 (2009).

[102] S. Yang and A. Navrotsky, Microporous Mesoporous Mater. **37**, 175 (2000).

[103] A. Navrotsky, Proc. Natl. Acad. Sci. USA. **101**, 12096 (2004).

[104] C.S. Cundy and P.A. Cox, Microporous Mesoporous Mater. **82**, 1 (2005).

[105] J.M. Fedeyko, D.G. Vlachos and R.F. Lobo, Langmuir **21**, 5197 (2005).

[106] S. Mintova, N.H. Olson, V. Valtchev and T. Bein, Science **283**, 958 (1999).

[107] S. Mintova, N.H. Olson and T. Bein, Angew. Chem. Int. Ed. **38**, 3201 (1999).

[108] J.C.G. Pereira, C.R.A. Catlow and G.D. Price, J. Phys. Chem. A. **103**, 3252 (1999).

[109] J.C.G. Pereira, C.R.A. Catlow and G.D. Price, J. Phys. Chem. A. **103**, 3268 (1999).

[110] C.S. Yang, J.M. Mora-Fonz and C.R.A. Catlow, J. Phys. Chem. C. **116**, 22121 (2012).

[111] M.C. Barnes, J. Addai-Mensah and A.R. Gerson, Microporous Mesoporous Mater. **31**, 287 (1999).

[112] W. Fan, S. Shirato, F. Gao, M. Ogura and T. Okubo, Microporous Mesoporous Mater. **89**, 227 (2006).

[113] H. Greer, P.S. Wheatley, S.E. Ashbrook, R.E. Morris and W.Z. Zhou, J. Am. Chem. Soc. **131**, 17986 (2009).

[114] A. Erdem and L.B. Sand, J. Catal. **60**, 241 (1979).

[115] T.T. Trinh, A.P.J. Jansen and R.A. van Santen, J. Phys. Chem. B. **110**, 23099 (2006).

[116] R.R. Holmes, Chem. Rev. **96**, 927 (1996).

[117] T.T. Trinh, A.P.J. Jansen, R.A. van Santen and E.J. Meijer, Phys. Chem. Chem. Phys. **11**, 5092 (2009).

[118] T.T. Trinh, A.P.J. Jansen, R.A. van Santen and E.J. Meijer, J. Phys. Chem. C. **113**, 2647 (2009).

[119] T.T. Trinh, A.P.J. Jansen, R.A. van Santen, J. VandeVondele and E.J. Meijer, ChemPhysChem. **10**, 1775 (2009).
[120] A. Pavlova, T.T. Trinh, R.A. van Santen and E.J. Meijer, Phys. Chem. Chem. Phys. **15**, 1123 (2012).
[121] J.C.G. Pereira, C.R.A. Catlow and G.D. Price, J. Phys. Chem. A. **106**, 130 (2002).
[122] B. Szyja, A. Jansen, T. Verstraelen and R. van Santen, Phys. Chem. Chem. Phys. **11**, 7605 (2009).
[123] T. Verstraelen, B.M. Szyja, D. Lesthaeghe, R. Declerck, V. Van Speybroeck, M. Waroquier, A.P.J. Jansen, A. Aerts, L.R.A. Follens, J.A. Martens, C.E.A. Kirschhock and R.A. van Santen, Top. Catal. **52**, 1261 (2009).
[124] B.M. Szyja, E.J.M. Hensen and R.A. van Santen, Catal. Today. **169**, 156 (2011).
[125] B.M. Szyja, P. Vassilev, T.T. Trinh, R.A. van Santen and E.J.M. Hensen, Microporous Mesoporous Mater. **146**, 82 (2011).
[126] R.M. Shayib, N.C. George, R. Seshadri, A.W. Burton, S.I. Zones and B.F. Chmelka, J. Am. Chem. Soc. **133**, 18728 (2011).
[127] F. Devreux, J.P. Boilot, F. Chaput and A. Lecomte, Phys. Rev. A **41**, 6901 (1990).
[128] L. Jin, S.M. Auerbach and P.A. Monson, J. Chem. Phys. **134**, 134703 (2011).
[129] N.Z. Rao and L.D. Gelb, J. Phys. Chem. B. **108**, 12418 (2004).
[130] S.H. Garofalini and G. Martin, J. Phys. Chem. **98**, 1311 (1994).
[131] G.J. McIntosh, Phys. Chem. Chem. Phys. **15**, 17496 (2013).
[132] X.Q. Zhang, T.T. Trinh, R.A. van Santen and A.P.J. Jansen, J. Am. Chem. Soc. **133**, 6613 (2011).
[133] X.Q. Zhang, T.T. Trinh, R.A. van Santen and A.P.J. Jansen, J. Phys. Chem. C. **115**, 9561 (2011).
[134] J. Šefčik and A.V. McCormick, Catal. Today. **35**, 205 (1997).
[135] X.Q. Zhang, R.A. van Santen and A.P.J. Jansen, Phys. Chem. Chem. Phys. **14**, 11969 (2012).
[136] S. Nangia and B.J. Garrison, J. Phys. Chem. A **112**, 2027 (2008).
[137] S. Nangia and B.J. Garrison, J. Am. Chem. Soc. **131**, 9538 (2009).
[138] S. Nangia and B.J. Garrison, J. Phys. Chem. C. **114**, 2267 (2010).
[139] S. Nangia and B.J. Garrison, Theor. Chem. Acc. **127**, 271 (2010).
[140] S. Nangia, N.M. Washton, K.T. Mueller, J.D. Kubicki and B.J. Garrison, J. Phys. Chem. C. **111**, 5169 (2007).
[141] M.G. Wu and M.W. Deem, J. Chem. Phys. **116**, 2125 (2002).
[142] R. Pophale, P.A. Cheeseman and M.W. Deem, Phys. Chem. Chem. Phys. **13**, 12407 (2011).
[143] R. Pophale, F. Daeyaert and M.W. Deem, J. Mater Chem. A. **1**, 6750 (2013).
[144] J.E. Schmidt, M.W. Deem and M.E. Davis, Angew. Chem. Int. Ed. **53**, 8372 (2014).
[145] M.H. Ford, S.M. Auerbach and P.A. Monson, J. Chem. Phys. **121**, 8415 (2004).
[146] M. Jorge, S.M. Auerbach and P.A. Monson, J. Am. Chem. Soc. **127**, 14388 (2005).
[147] A. Malani, S.M. Auerbach and P.A. Monson, J. Phys. Chem. Lett. **1**, 3219 (2010).
[148] A. Malani, S.M. Auerbach and P.A. Monson, J. Phys. Chem. C. **115**, 15988 (2011).
[149] M. Jorge, S.M. Auerbach and P.A. Monson, Mol. Phys. **104**, 3513 (2006).
[150] L. Jin, S.M. Auerbach and P.A. Monson, J. Phys. Chem. C. **114**, 14393 (2010).
[151] L. Jin, S.M. Auerbach and P.A. Monson, J. Phys. Chem. Lett. **3**, 761 (2012).
[152] L. Jin, S.M. Auerbach and P.A. Monson, Langmuir **29**, 766 (2013).
[153] D.J. Earl and M.W. Deem, Abstr. Pap. Am. Chem. Soc. **237**, 1 (2009).
[154] F.R. Siperstein and K.E. Gubbins, Langmuir **19**, 2049 (2003).
[155] R.G. Larson, J. Chem. Phys. **91**, 2479 (1989).
[156] J.E. Magee and F.R. Siperstein, J. Phys. Chem. C. **113**, 1680 (2009).
[157] A. Patti, A.D. Mackie and F.R. Siperstein, Langmuir **23**, 6771 (2007).
[158] A. Patti, A.D. Mackie and F.R. Siperstein, J. Mater. Chem. **19**, 7848 (2009).
[159] A. Patti, A.D. Mackie, V. Zelenak and F.R. Siperstein, J. Mater. Chem. **19**, 724 (2009).

[160] A. Patti, F.R. Siperstein and A.D. Mackie, J. Phys. Chem. C. **111**, 16035 (2007).

[161] C. Schumacher, J. Gonzalez, P.A. Wright and N.A. Seaton, J. Phys. Chem. B. **110**, 319 (2006).

[162] S. Bhattacharya and K. Gubbins, J. Chem. Phys. **123**, 134907 (2005).

[163] B. Coasne, F. Hung, R. Pellenq, F. Siperstein and K. Gubbins, Langmuir **22**, 194 (2006).

[164] M. Jorge, J.R.B. Gomes, M.N.D.S. Cordeiro and N.A. Seaton, J. Am. Chem. Soc. **129**, 15414 (2007).

[165] M. Jorge, J.R.B. Gomes, M.N.D.S. Cordeiro and N.A. Seaton, J. Phys. Chem. B. **113**, 708 (2009).

[166] G. Pérez-Sánchez, J.R.B. Gomes and M. Jorge, Langmuir **29**, 2387 (2013).

[167] R.G. Larson, L.E. Scriven and H.T. Davis, J. Chem. Phys. **83**, 2411 (1985).

[168] D. Frenkel and B. Smit, *Understanding Molecular Simulation: From Algorithms to Applications*, 2nd ed. (Academic, San Diego, CA, 2002).

[169] N.K. Raman, M.T. Anderson and C.J. Brinker, Chem. Mater. **8**, 1682 (1996).

[170] W.R. Smith and B. Triska, J. Chem. Phys. **100**, 3019 (1994).

[171] J.Y. Zhang, Z. Luz and D. Goldfarb, J. Phys. Chem. B. **101**, 7087 (1997).

[172] R. Zana, J. Frasch, M. Soulard, B. Lebeau and J. Patarin, Langmuir. **15**, 2603 (1999).

[173] F.R. Siperstein and K.E. Gubbins, Mol. Sim. **27**, 339 (2001).

[174] M. Kruk, M. Jaroniec, Y. Sakamoto, O. Terasaki, R. Ryoo and C.H. Ko, J. Phys. Chem. B. **104**, 292 (2000).